



**POLITECNICO**  
MILANO 1863

SCUOLA DI INGEGNERIA INDUSTRIALE  
E DELL'INFORMAZIONE

## Development of a data-driven surrogate model for helium production in fast reactor Am-bearing fuels

**Advisor:**

Prof. Lelio Luzzi

**Co-advisors:**

Davide Pizzocri

Alessio Magni

**Academic year:**

2021-2022

**Abstract:** Helium production in the nuclear fuel matrix during irradiation plays a critical role in the design and performance of Generation IV reactor fuel, as it is a major limiting factor regarding fuel burnup. A surrogate model for helium production is developed by statistical analysis of synthetic datasets obtained from the SCIANTIX extended and verified burnup module using the Latin hypercube sampling method. The burnup module is verified against high-fidelity results from the SERPENT depletion code and validated against experimental results from SUPERFACT-1 and SPHERE irradiation experiments. The surrogate model calculates helium production rate in uranium-plutonium mixed oxide (MOX) fuel containing minor actinides (MA) and in particular americium, as a function of the reactor fission rate density and irradiation time. The model is designed to put emphasis on minimal computational cost for its envisaged application in fuel performance codes.

Keywords: MOX fuel, Am-bearing MOX, Helium production, Fast Reactors, Generation IV

### 1. Introduction

Developments in research regarding Generation IV fast reactors with minor actinide (MA)-bearing MOX<sup>1</sup> fuel, and the related fuel cycle technologies dictate a need in detailed understanding of its behavior under irradiation and in storage conditions. One important aspect of the behavior of MA-bearing fuel is the helium production in the fuel, migration through pores generated and transformed with burnup and eventual release into the fuel free volume, which affects numerous aspects of the nuclear fuel performance like the increase of pin internal pressure and the decrease in the fuel thermal conductivity [1].

This is due to the production of large amounts of relatively short-lived actinides in the fuel when MAs are included in its initial composition in comparison with conventional uranium-plutonium or uranium dioxide fuel. Such short-lived actinides as <sup>242</sup>Cm, <sup>244</sup>Cm and <sup>238</sup>Pu, decay through the (n,α) reaction during irradiation and storage conditions, producing more α particles (helium nuclei) than in the conventional fuel. A second path to produce helium in nuclear fuel is the <sup>16</sup>O (n,α) reaction with a threshold of neutron energy of ~4 MeV, and monotonously increasing for energy up to 10 MeV with an appreciable cross-section value of 0.26 barn [2]. As a result, the helium production rate is dependent on the energy distribution of fast neutrons (fast spectrum). The third path for helium production in nuclear fuel is ternary fission, with MA isotopes having relatively higher helium yield from fast fission compared to uranium and plutonium isotopes [3].

The standard tools applied to estimate helium production in the fuel, are fuel depletion codes that enable a reliable estimation of the concentration evolution of the various actinides contained within the fuel, along with

<sup>1</sup> The term MOX herein refers to (U,Pu)O<sub>2</sub> homogeneous fuel designed for fast reactor applications.

validation data obtained from experimental campaigns like SPHERE [4], SUPERFACT [5], MARIOS [6]. In addition, fuel performance codes devoted to the prediction of the thermo-mechanical behavior of the fuel pin require the predictive capability of tracking the evolution of the fuel composition with burnup. These codes use either dedicated burnup module packages like the TUBRNP module for the TRANSURANUS code [7], or standalone helium production correlations [8,9]. Each of these methods have their respective advantages and disadvantages with burnup modules having greater accuracy at the expense of an increased computational cost and standalone correlations being less accurate and specific to certain fuel/reactor combinations [10], but fast running making them more suitable to implement in existing fuel performance codes when many iterations are needed to be performed in separate positions if the fuel matrix.

In depletion calculations, the solution of neutron transport is the main step which renders fast running calculations impractical. Monte Carlo depletion codes have been developed which track the rates of change of the isotope inventory of the nuclear fuel with high accuracy and fidelity [11,12], by considering the sequential steady state neutronics solution at each burnup step to reduce computational times. To this end, codes such as SCALE [13] employ access to microscopic cross-section libraries, with multidimensional matrices determining the dependence of the cross-sections on incident neutron energy and angle.

Burnup modules within fuel performance codes have thus been developed, which are computationally less expensive but with a reduced application range. Nonetheless, they account for the macroscopic cross-section dependence on the fuel composition and the reactor type (i.e., boiling water reactor (BWR), pressurized water reactor (PWR), sodium-cooled fast reactor (SFR) or lead-cooled fast reactor (LFR)). Different procedures have been used for the implementation of the effective macroscopic cross-sections' sets, based on the initial fuel composition and End of Life (EoL) burnup requirements without any standardized methodology for generating them [14-16]. The TUBRNP module embedded in the TRANSURANUS fuel performance code, uses effective cross-sections for neutron-induced fissions and captures in  $\text{UO}_2$  fuel that depend the reactor type and on the enrichment of  $^{235}\text{U}$ , while the related cross-sections for liquid water reactors (LWR) MOX fuel depend on the initial plutonium concentration [17]. In the SCIENTIX burnup module embedded in the SCIENTIX code, the effective-cross section calculations are performed in a similar fashion and depend on plutonium enrichment and burnup level of the fuel [18]. Additional burnup modules include RAPID [19], RTOP [20] and the DIONISIO code [21].

Regarding helium production correlations, Akie et al. 2013 [22] proposed a simple mechanistic formula for helium production which considers the three main pathways of helium production inside the fuel, verified it with the high-fidelity results of the SWAT code, and validated it against experimental data produced at the JOYO fast reactor. Recently, Tarasov and coauthors [23], modified the BONUS model to describe helium and hydrogen behavior in irradiated fuels and implemented it in the MFPR/R, SFPR and BERKUT-U fuel rod codes.

In this work the SCIENTIX burnup module is used in tandem with the SERPENT Monte Carlo code [24] to generate the macroscopic cross-section tables for two relevant fuel/reactor combinations. First the existing burnup module [18] is verified against high-fidelity SERPENT results in the intermediate points of the defined look-up tables for two cases regarding MOX fuel in fast reactor conditions: a sodium cooled fast reactor and a lead bismuth eutectic-cooled fast reactor. Subsequently, the SCIENTIX burnup module is extended to a finer grid of burnup and plutonium enrichment steps, also regarding plutonium content up to 51%. In Section 2.1 and 2.2 the general overview of the burnup module is given as well as the methodology employed. In Section 2.3 the verification results are presented along with the validation of the extended burnup module with the experimental data from SUPERFACT-1 and SPHERE irradiation experiments.

Subsequently, the extended burnup module is used to generate synthetic datasets covering a wide range of input variables regarding the initial composition of MA-bearing fuel and its thermophysical properties, and a helium production surrogate model is developed based on non-linear multivariate regression performed on the datasets. The proposed correlation is intended to be used as a fast-running standalone package implemented in fuel performance codes with focus on reduced computational loads with respect to the burnup module, that enables multiple calculations to be performed iteratively. In Section 2.4 the methodology following this procedure is explained in detail, and the verification results are presented in Section 2.5.

## 2.1 Description of the SCIANTIX burnup module

The SCIANTIX code is a zero-dimensional code developed at Politecnico di Milano and is designed to be used both as a stand-alone code to validate fission gas behavior models or coupled with existing fuel performance codes [25,26]. It can be implemented in fuel performance codes and multi-physics platforms as an externally assessed module to evaluate fission gas release, gaseous swelling, and nuclides evolution. The numerical solvers of SCIANTIX, function in separate modules from the system physics, enabling numerical verification. The code offers no user interface, and all information exchange is performed through the input and output files. The input files consist of the *input initial conditions*, a catalog of initial condition related to the initial fuel composition, the *input settings*, a set of integer values that setup the simulation main parameters (e.g., determining the correlations to be used, the fuel/reactor combination etc.), and the *input history* file which contains information about the evolution in time, the corresponding fission rate density and fuel temperature to define a grid of points on which the calculations will be performed.

The SCIANTIX burnup module accounts for helium production via three main routes:  $(n,\alpha)$  reactions of  $^{16}\text{O}$ ,  $\alpha$ -decays of short-lived transuranic elements, and ternary fissions. The uranium isotopes included in the burnup module are  $^{234}\text{U}$ ,  $^{235}\text{U}$ ,  $^{236}\text{U}$ ,  $^{237}\text{U}$  and  $^{238}\text{U}$ . Despite  $^{233}\text{U}$  being a component of  $\text{UO}_2$  and MOX fuels, it is not treated by the module as it belongs to the neptunium  $4n+1$  series, and undergoes  $\alpha$ -decay into  $^{229}\text{Th}$ , and subsequently to lighter nuclei. Furthermore,  $^{233}\text{U}$  is produced from  $^{233}\text{Pa}$   $\beta$ -decay, which is in turn produced from the  $\alpha$ -decay of  $^{237}\text{Np}$  with a half-life ( $t_{1/2}$ ) of 2.144 million years. Apart from its limited production rate,  $^{233}\text{U}$  has a long half-life of  $\alpha$ -decay at 159.2 thousand years, so it is excluded from the depletion calculations.  $^{239}\text{U}$  is produced by  $(n,\gamma)$  reaction with  $^{238}\text{U}$ , undergoes  $\beta$ -decay into  $^{239}\text{Np}$  with a half-life of 26.6 minutes and subsequently into  $^{239}\text{Pu}$ . Due to the short decay time in comparison with the other uranium isotopes, it is also excluded from the depletion chain under the approximation that it is instantaneously converted into  $^{239}\text{Np}$ .

The included plutonium isotopes are  $^{238}\text{Pu}$ ,  $^{239}\text{Pu}$ ,  $^{240}\text{Pu}$ ,  $^{241}\text{Pu}$ ,  $^{242}\text{Pu}$  and  $^{243}\text{Pu}$ . Despite the short half-life of  $^{243}\text{Pu}$  ( $t_{1/2} = 4.95\text{h}$ ), it is included in the module because it is transmuted into  $^{243}\text{Am}$  which is an  $\alpha$ -emitter and relevant in the helium concentration evolution.

The module also tracks the minor actinides concentration evolution such as neptunium, americium, and curium isotopes. The included neptunium isotopes are  $^{237}\text{Np}$ ,  $^{238}\text{Np}$ , and  $^{239}\text{Np}$ .  $^{240}\text{Np}$  is produced only from the  $(n,\gamma)$  reaction of  $^{239}\text{Np}$  with subsequently decays by  $\beta$ -decay into  $^{239}\text{Pu}$  with a half-life of 2.356 days. Due to its relatively short decay time, it is excluded from the depletion calculations. Regarding americium isotopes those included in the module are  $^{241}\text{Am}$ ,  $^{242}\text{Am}$ ,  $^{242\text{m}}\text{Am}$ ,  $^{243}\text{Am}$  and  $^{244}\text{Am}$ . The metastable state of  $^{242}\text{Am}$  undergoes  $\beta$ -decay into  $^{242}\text{Cm}$  with a half-life of 141 years and is important for the production rate of helium in the fuel [27]. The included curium isotopes are  $^{242}\text{Cm}$ ,  $^{243}\text{Cm}$ ,  $^{244}\text{Cm}$  and  $^{245}\text{Cm}$ . Botazzoli [28] demonstrated that satisfactory description of helium concentration evolution due to  $\alpha$ -decays can be achieved by considering the evolution of transuranic elements up to  $^{245}\text{Cm}$  in the scope of fuel performance codes' calculations.

In addition to the  $\alpha$  and  $\beta$  decay of each nuclide, the burnup module also considers the internal transition of  $^{242\text{m}}\text{Am}$  and the electron capture of  $^{242}\text{Am}$ . Decay processes with branching ratios lower than the 1% threshold are excluded. Furthermore,  $(n,2n)$  and  $(n,3n)$  neutron multiplication reactions, as well as fission reactions and radiative captures are included, with the significance of each reaction group being apparent for different reactor operating conditions (e.g., for thermal reactors the fission reaction cross-sections are higher than fast reactors, and neutron multiplication reactions have higher cross-sections in fast reactor conditions). In this work the  $(n,2n)$  reactions of  $^{238}\text{U}$ ,  $^{241}\text{Pu}$ ,  $^{243}\text{Pu}$ ,  $^{242}\text{Am}$ ,  $^{242\text{m}}\text{Am}$  and  $^{245}\text{Cm}$  have been added to the burnup module to improve its predictive ability, with a relatively small computational cost of 3% increase in computational time, consistent with the requirements of industrial fuel performance codes.

The resulting equation for the helium production rate in the SCIANTIX burnup module, is thus formulated as:

$$\begin{aligned}
 \frac{d[{}^4\text{He}]}{dt} = & \lambda_{\alpha,234\text{U}} [{}^{234}\text{U}] + \lambda_{\alpha,235\text{U}} [{}^{235}\text{U}] + \lambda_{\alpha,236\text{U}} [{}^{236}\text{U}] + \lambda_{\alpha,238\text{U}} [{}^{238}\text{U}] \\
 & + \lambda_{\alpha,237\text{Np}} [{}^{237}\text{Np}] \\
 & + \lambda_{\alpha,238\text{Pu}} [{}^{238}\text{Pu}] + \lambda_{\alpha,239\text{Pu}} [{}^{239}\text{Pu}] + \lambda_{\alpha,240\text{Pu}} [{}^{240}\text{Pu}] + \lambda_{\alpha,242\text{Pu}} [{}^{242}\text{Pu}] \\
 & + \lambda_{\alpha,241\text{Am}} [{}^{241}\text{Am}] + \lambda_{\alpha,243\text{Am}} [{}^{243}\text{Am}] \\
 & + \lambda_{\alpha,242\text{Cm}} [{}^{242}\text{Cm}] + \lambda_{\alpha,243\text{Cm}} [{}^{243}\text{Cm}] + \lambda_{\alpha,244\text{Cm}} [{}^{244}\text{Cm}] + \lambda_{\alpha,245\text{Cm}} [{}^{245}\text{Cm}] \\
 & + \sigma_{(n,\alpha),{}^{16}\text{O}} \varphi [{}^{16}\text{O}] + y_{TF} \dot{F}
 \end{aligned} \tag{2.1}$$

where  $[^iX]$  (at  $m^{-3}$ ) is the concentration of the nuclide  $^iX$ ,  $\lambda_{\alpha, ^iX}$  ( $s^{-1}$ ) is the  $\alpha$ -decay constant of the nuclide  $^iX$ ,  $\sigma_{(n,\alpha),^{16}O}$  ( $m^2$ ) is the  $(n,\alpha)$  reaction cross-section of  $^{16}O$ ,  $\varphi$  ( $m^{-2} s^{-1}$ ) is the local neutron flux,  $y_{TF}$  is the ternary fission yield which is equal to 0.22% [29], and  $\dot{F}$  ( $m^{-3} s^{-1}$ ) is the local fission rate density.

Twenty-three actinides are included in the burnup module, with a resulting set of Bateman equations to be solved (Appendix A).

At each time step, a two-step procedure is performed. Initially, the cross-section values for each nuclear reaction type regarding all nuclides are calculated from look-up tables based on the local burnup and initial fuel composition via an interpolation algorithm. Subsequently, the numerical integration of the Bateman equations is performed via a Backward Euler numerical scheme, and the fuel composition including helium (Eq. 2.1) at the end of the time step is used as input for the next calculation interval. Decoupling the solution of the Bateman equations from the cross-sections' calculations simplifies the solution procedure, but the dependence of each fuel/reactor combination on the specific cross-section lookup table is made evident. By increasing the integration points, the error decreases while the execution time of the model increases [30,31]. The microscopic cross-section corresponding to a target burnup  $bu_{target}$  and enrichment  $e_{target}$  coordinate lies between four discrete burnup/enrichment points on the SERPENT-defined lookup table, and is calculated by:

$$\begin{aligned} {}^iX\bar{\sigma}_r(e_{target}, bu_{target}) &= {}^iX\bar{\sigma}_r(e_1, bu_1) A_{22} + {}^iX\bar{\sigma}_r(e_1, bu_2) A_{21} \\ &+ {}^iX\bar{\sigma}_r(e_2, bu_1) A_{12} + {}^iX\bar{\sigma}_r(e_2, bu_2) A_{11} \end{aligned} \quad (2.2)$$

where  $A_{ij}$  are the respective weights of the four lookup table values calculated by:

$$A_{ij} = \left| (e_{target} - e_i) \cdot (bu_{target} - bu_j) \right| \quad (2.3)$$

The local neutron flux is calculated by:

$$\bar{\varphi} = \frac{\dot{F}}{\bar{\Sigma}_f} \quad (2.4)$$

where  $\bar{\Sigma}_f$  ( $m^{-1}$ ) is the approximated one-group macroscopic cross-section for fission calculated over  $n$ -fissile nuclides as:

$$\bar{\Sigma}_f = \sum_n {}^nX\bar{\sigma}_f[{}^nX](t_n) \quad (2.5)$$

where  ${}^nX\bar{\sigma}_f[{}^nX](m^2)$  is the fission microscopic cross-section of the nuclide  ${}^nX$ . Given the cross-section values, the Bateman equations are solved independently as a linear ordinary differential equations (ODE) system:

$$\frac{d[X]_i}{dt} = \sum_{rj} {}^iX\bar{\sigma}(e_0, bu) \bar{\varphi}[{}^jX] - \sum_r {}^iX\bar{\sigma}(e_0, bu) \bar{\varphi}[{}^iX] + \sum_{dk} \lambda_{d,k} [{}^kX] - \sum_d \lambda_{d,i} [{}^iX] \quad (2.6)$$

where the first summation term describes the production of the  ${}^iX$ -nuclide resulting from the  $r$ -reaction of the  ${}^jX$ -nuclide, the second summation term describes the  $r$  transmutation of the  ${}^iX$ -nuclide due to the  $r$ -reaction, the third summation term describes the production of the  ${}^iX$ -nuclide from the decay  $d$  of the  ${}^kX$ -nuclide, and the fourth summation term describes the decay  $d$  of the  ${}^iX$ -nuclide. The ODE-system is solved with the Backward-Euler method, consistent with the numerical framework established in the SCIENTIX code.

## 2.2 Methodology of the extension and verification of the SCIANTIX burnup module

The methodology used in this work to extend the SCIANTIX burnup module follows a standardized development procedure, regarding a user-specified fuel/reactor combination, and can be summarized as follows:

- A set of SERPENT simulations is performed for an initial fuel composition vector, corresponding to the fuel/reactor combination under evaluation.
- For each initial composition step  $e_i$ , and each burnup step  $bu_i$ , the respective cross-section values are extracted, evaluated by the reaction rate integrals (RRI) in the SERPENT simulation.
- An  $e_i$  by  $bu_i$  matrix is created containing the microscopic cross-section values, with each row representing the initial enrichment steps and each column the burnup steps for each nuclide and each reaction type.
- The matrices are implemented in the SCIANTIX burnup module as lookup tables corresponding to the relevant fuel/reactor combination.

This procedure occurs once and for all, and the produced look-up tables are incorporated once in the SCIANTIX burnup module. The user can then dictate the choice of the respective lookup tables corresponding to the fuel/reactor combination to simulate. Subsequently, the SCIANTIX calculations are performed, the cross sections on the intermediate points of the enrichment x burnup grid being calculated by interpolation (Fig 2.3). To produce the cross-section tables, SERPENT calculates the reaction rates specified by the user, integrated over space and energy (RRI) by using the collision estimate of neutron flux [33]:

$$R = \frac{1}{V} \iint_{V E} f(\mathbf{r}, E') \varphi(\mathbf{r}, E') d^3r dE' \quad (2.7)$$

where  $V(\text{m}^3)$  is the volume of the target material,  $E(\text{eV})$  is the energy grid defined by the user,  $f(\mathbf{r}, E')$  is the required response function, and  $\varphi(\mathbf{r}, E')$  ( $\text{m}^{-2} \text{s}^{-1} \text{eV}^{-1}$ ) is the space and incident neutron energy-dependent neutron flux. To obtain the absolute value of the RRI, SERPENT considers a user-defined source normalization term. In this work a specific power of  $40 \text{ kW kg}^{-1}$ , (208 MeV per fission are assumed as conversion factor between the specific power and the fission rate). The microscopic cross sections for each nuclide and each nuclear reaction (response function) are then calculated by:

$${}^i_x \bar{\sigma}_r(e_0, bu) = \frac{\iint_{V E} {}^i_x \sigma_r^i(e_0, bu, E') \varphi(\mathbf{r}, E') d^3r dE'}{\iint_{V E} \varphi(\mathbf{r}, E') d^3r dE'} \quad (2.8)$$

where  ${}^i_x \bar{\sigma}_r(e_0, bu, E')$  is the cross section of the  $r$ th nuclear reaction of the  $i$ th nuclide as a function of the initial plutonium enrichment  $e_0$ , the burnup step  $bu$  and the incident neutron energy  $E'$ . The SERPENT depletion calculation adopts a Chebyshev Rational Approximation Method (CRAM) for the decomposition and solution of the system determined by the burnup matrix [34]. A predictor-corrector algorithm (PCC) is used for each calculation node, with linear extrapolation occurring in the predictor step for time integration and linear interpolation occurring in the corrector step. An initial neutron population of 10000 neutrons is used, with 100 active and 30 inactive cycles which facilitates reasonable computational times with relatively low standard deviation [33]. Two fast reactor cases have been simulated, a Sodium cooled Fast Reactor (SFR) and the Liquid Bismuth Eutectic cooled Fast Reactor (LBE-FR). The simulation domain of the SERPENT code consists of a single fuel pin with cylindrical geometry, composed of the uniform fuel pellet, the fuel-cladding gap and the cladding, encompassed by the respective coolant material. The simulation universe is a cube of side length equal to the fuel pin length. The boundary condition at the end-surfaces of the SERPENT defined simulation universe is reflective [33]. The fuel composition (dependent on the initial plutonium enrichment) and the

cladding composition (15-15 Ni-Cr, Ti-stabilized, stainless steel (SS)) are adopted by the French SFR [35]. The specifications for SERPENT simulation are collected in Table 2.1.

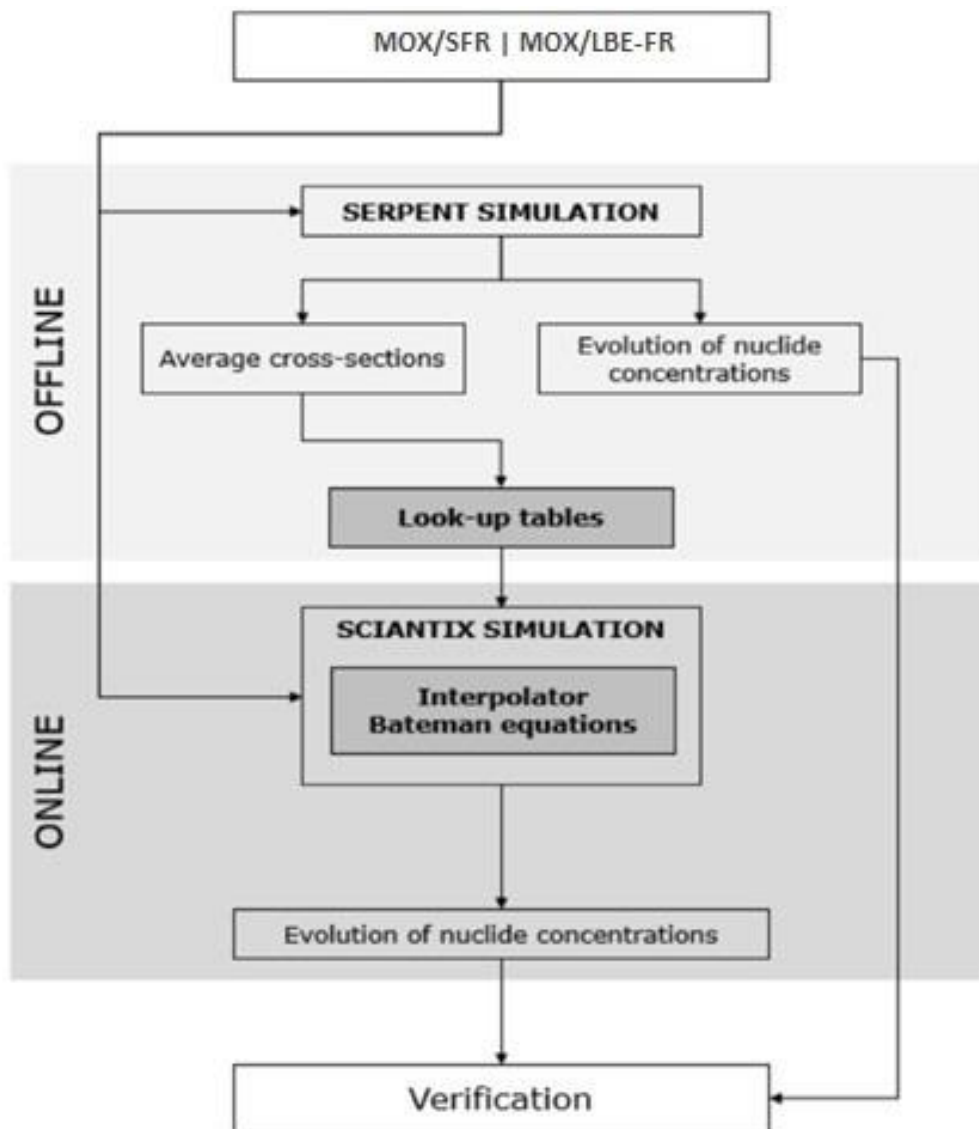


**Fig 2.3.** Standardized methodology applied for the generation of the cross-section look-up table for the corresponding fuel/reactor combination. SERPENT simulations are performed OFFLINE, while the SCIENTIX simulations are performed ONLINE. (Source: Cechet et al. 2021 [18]).

**Table 2.1.** Specifications of the SERPENT simulations for the two fuel/reactor combinations. Each calculated cross section value corresponds to a set of burnup and enrichment node.

Parameter	MOX/SFR	MOX/LBE-FR
External pellet radius (mm)	2.71	2.71
Radial gap (mm)	0.116	0.116
U/HM (%)	80-49 <sup>a</sup>	80-49 <sup>a</sup>
Pu/HM (%)	20-51 <sup>b</sup>	20-51 <sup>b</sup>
Enrichment step width (at/HM %)	1	1
O/HM ratio	1.957	1.957
Fuel density (kg m <sup>-3</sup> )	10970	10970
Column length (mm)	850	850
Cladding material	15-15 Ni-Cr, Ti-stabilized SS	15-15 Ni-Cr, Ti-stabilized SS
Cladding thickness	0.45	0.45
Cladding density (kg m <sup>-3</sup> )	7950	7950
Coolant	Sodium	Lead - Bismuth Eutectic (Pb 45 wt%, Bi 55 wt%)
Simulation universe side length(mm)	870	870
Coolant density (kg m <sup>-3</sup> )	610	10280
Total burnup (GWd/t <sub>HM</sub> )	200	200
Burnup step width (GWd/t <sub>HM</sub> )	2.5	2.5
Burnup steps	81	81
Fission rate density (fiss m <sup>-3</sup> s <sup>-1</sup> )	1.32·10 <sup>19</sup>	1.32·10 <sup>19</sup>

<sup>a</sup> Natural uranium composition.

<sup>b</sup> <sup>238</sup>Pu 1.3 wt. %, <sup>239</sup>Pu 60.4 wt. %, <sup>240</sup>Pu 23.4 wt.%, <sup>241</sup>Pu 10.4 wt.%, <sup>242</sup>Pu 4.5 wt.%.

To quantify the predictive capability of the updated SCIANTIX burnup module of the nuclides' concentration the Root-Mean Square Error (RMSE) has been calculated as a verification metric by:

$$RMSE = \sqrt{\frac{1}{N} \sum_{n=1}^N \left( \frac{C_n - R_n}{R_n} \right)^2} \quad (2.9)$$

where  $C_n$  is the burnup module calculated value,  $R_n$  is the SERPENT reference value and  $N$  is the number of burnup steps.

In the first part of this work the predictive capability of the existing burnup module (Cechet et al. 2021, [18]), was quantified for intermediate values of burnup and enrichment with respect to the lookup table definition values. For this reason, the depletion calculation was performed in 81 equally distanced burnup steps of 2.5 GWd/t<sub>HM</sub> up to 200 GWd/t<sub>HM</sub> and 31 plutonium enrichment (Pu/HM) steps starting from 20 up to 51%. Subsequently, the extended lookup table obtained from SERPENT was implemented in the SCIANTIX burnup module and the results were verified against the high-fidelity SERPENT results as depicted in Section 2.3. The specifications of the SCIANTIX simulations are shown in Table 2.2.

**Table 2.2.** Specifications for the SCIANTIX simulations for the two fuel/reactor combinations.

Parameter	MOX/SFR	MOX/LBE-FR
Number of history points	81	81
Number of time steps per history point	1000	1000
Irradiation time (h)	120000	106000
Burn-up at discharge (GWd/t <sub>HM</sub> )	226	200
Fission rate density (fiss m <sup>-3</sup> s <sup>-1</sup> )	1.32·10 <sup>19</sup>	1.17·10 <sup>19</sup>
Grain radius (m)	10·10 <sup>-6</sup>	10·10 <sup>-6</sup>
Fuel density (kg m <sup>-3</sup> )	10970	10970
O/HM ratio	1.957	1.957
Execution time (s)	41.72	39.23

### 2.3 Verification of the SCIANTIX burnup module

The SCIANTIX burnup module (Cechet et al. 2021, [18]) is verified against the high-fidelity SERPENT results in the intermediate values of the lookup table definition points, to test the error introduced by the interpolation algorithm. As the lookup tables are defined for Pu/HM values from 20 to 40% with a step of 2% and burnup steps of 5 GWd/t<sub>HM</sub> (0, 5, 10,...200 GWd/t<sub>HM</sub>), the module was verified against SERPENT predictions calculated at Pu/HM values of 21 to 51% with steps of 2% and burnup values of 0, 2.5, 7.5,...200GWd/t<sub>HM</sub>. The verification was performed for 31 initial enrichment steps for each of the 22 nuclides, and for the two fuel/reactor combination cases. A schematic representation of the verification grids used in the work of Cechet et al. 2021 [18] and this work is shown in Fig. 2.4. Due to the large amount of data generated, only the results of one enrichment level (31%) are herein presented.

A comparison of the RMSE (averaged in burnup) is depicted in Figs. 2.5-2.8 for the SFR, for four enrichment cases 21%, 31%, 41%, and 51%. It is evident that the RMSE of the extended burnup module is consistently lower, for all enrichment levels, with deviation for the two modules for enrichment values higher than 40% as it is beyond the definition points of the lookup tables of the existing burnup module. The average RMSE for all plutonium enrichment steps is shown in Fig. 2.9, where it is evident that the extended burnup module has a consistently better predictive performance compared to the previous version, albeit with a small margin for enrichments up to 41% where the margin increases significantly. The decrease of the burnup module's performance can be attributed to the effect of higher values of burnup that the increased content in fissile plutonium material has on the simulation bounds. Indeed, for high plutonium content, for the same fission rate density, the final burnup at the fuel end-of-life was 226 GWd/t<sub>HM</sub> which is out of the defined lookup table bounds for both versions of the burnup module. It is important to note that the existing burnup module performs sufficiently well for burnup and enrichment values in the intermediate points of the lookup tables' definition. In Table 2.3, the RMSE values of all nuclides for each enrichment level for the SFR case are collected.

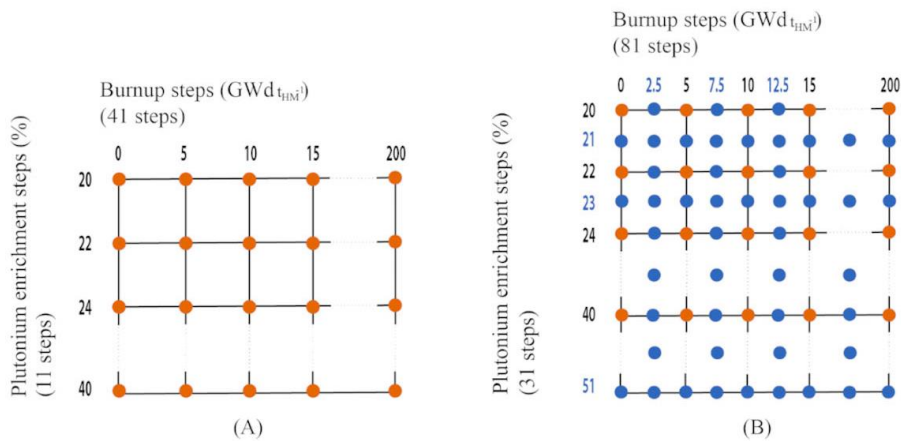


**Fig 2.4.** Burnup/enrichment grid used for verification of the SCIANTIX burnup module against SERPENT (blue, this work; orange, Cechet et al. 2021 [18], i.e., previous version of the module itself).

**Table 2.3. RMSE values for all the plutonium enrichment steps for all nuclides in the SFR case.**

RMSE	21% Pu		23% Pu		25% Pu		27% Pu		29% Pu		31% Pu		33% Pu		35% Pu		37% Pu		39% Pu	
	MOX/SFR UPDATED	MOX/SFR OLD																		
	81x16	41x11																		
U234 (at/m3)	0.061743	0.08215	0.062938	0.078824	0.059582	0.075507	0.057359	0.072461	0.055031	0.069431	0.052751	0.066458	0.050734	0.063541	0.048684	0.060846	0.046725	0.058269	0.044905	0.05574
U235 (at/m3)	0.119815	0.141723	0.11703	0.134924	0.112148	0.128548	0.107585	0.122712	0.10305	0.116853	0.098729	0.111463	0.094574	0.106212	0.090606	0.101411	0.086691	0.096943	0.083014	0.092473
U236 (at/m3)	0.034258	0.069558	0.051398	0.072253	0.053177	0.075059	0.055045	0.077678	0.056681	0.079975	0.0584	0.082496	0.059695	0.084033	0.061072	0.085765	0.061957	0.087388	0.062768	0.088339
U237 (at/m3)	0.14749	0.173732	0.149828	0.176277	0.146422	0.17913	0.1462	0.179489	0.149567	0.178427	0.158609	0.180165	0.148301	0.176693	0.151053	0.176275	0.159436	0.179126	0.155055	0.184804
U238 (at/m3)	0.018135	0.017087	0.017645	0.016525	0.01691	0.015974	0.016255	0.015446	0.015601	0.014917	0.015003	0.014432	0.014406	0.013944	0.013825	0.013503	0.01328	0.013074	0.012752	0.012642
Np237 (at/m3)	0.098155	0.094467	0.08238	0.093309	0.089813	0.10115	0.08364	0.10346	0.094604	0.097277	0.095832	0.103669	0.090126	0.096845	0.09112	0.094328	0.093547	0.100866	0.095432	0.106128
Np238 (at/m3)	0.233395	0.308951	0.250943	0.307425	0.245583	0.313814	0.240537	0.315014	0.249948	0.306759	0.253182	0.311975	0.24514	0.304069	0.246914	0.300831	0.250602	0.3066	0.250871	0.312178
Np239 (at/m3)	0.101455	0.097354	0.102124	0.098464	0.103049	0.09978	0.104774	0.101661	0.105791	0.102936	0.10742	0.104706	0.108965	0.106588	0.1110257	0.108636	0.111655	0.110765	0.112885	0.112527
Pu238 (at/m3)	0.040364	0.038722	0.039612	0.039645	0.040151	0.040056	0.039822	0.040219	0.039191	0.040151	0.038287	0.039673	0.037606	0.039101	0.036573	0.038351	0.035531	0.037498	0.034549	0.036810
Pu239 (at/m3)	0.028024	0.049927	0.035093	0.049664	0.034752	0.049544	0.036119	0.049626	0.037512	0.049692	0.038772	0.049751	0.039901	0.049901	0.040975	0.049889	0.04183	0.04986	0.042582	0.049769
Pu240 (at/m3)	0.00488	0.008165	0.003522	0.006058	0.005488	0.004528	0.006545	0.003744	0.007464	0.003512	0.008123	0.00369	0.008678	0.003938	0.009029	0.004214	0.009282	0.004408	0.009356	0.004615
Pu241 (at/m3)	0.004881	0.05088	0.018797	0.045224	0.010952	0.040155	0.009373	0.036153	0.007957	0.032453	0.006973	0.029433	0.006246	0.026756	0.005613	0.024653	0.005197	0.022628	0.004885	0.020869
Pu242 (at/m3)	0.016745	0.025248	0.015658	0.02514	0.015764	0.024885	0.015795	0.024267	0.015709	0.0236	0.01553	0.022853	0.015283	0.022027	0.015015	0.021381	0.014665	0.020781	0.014324	0.020125
Am241 (at/m3)	0.071693	0.058398	0.068341	0.059994	0.065486	0.060878	0.064752	0.061231	0.063846	0.061115	0.062597	0.060648	0.061271	0.059953	0.05982	0.058987	0.058279	0.05798	0.056735	0.056810
Am242 (at/m3)	0.051465	0.119762	0.081918	0.116106	0.074534	0.113662	0.075541	0.112539	0.076222	0.111334	0.07752	0.110977	0.078918	0.110916	0.080684	0.111545	0.082079	0.112268	0.083699	0.112964
Am243 (at/m3)	0.049562	0.158775	0.072758	0.158202	0.072594	0.158992	0.075174	0.15984	0.077395	0.15974	0.079877	0.159365	0.08188	0.15933	0.08462	0.160958	0.086491	0.163036	0.088512	0.164176
Am242m (at/m3)	0.233243	0.269558	0.254159	0.271278	0.255827	0.273559	0.258124	0.276054	0.259955	0.278202	0.262132	0.280534	0.263686	0.282375	0.265739	0.284544	0.267466	0.286716	0.269168	0.288783
Cm242 (at/m3)	0.154568	0.198234	0.174753	0.196722	0.172746	0.196223	0.173708	0.196409	0.174403	0.19653	0.175546	0.197097	0.176315	0.197538	0.177597	0.198441	0.178705	0.199515	0.179843	0.200552
Cm243 (at/m3)	0.836437	1.086192	0.923517	1.089863	0.931952	1.095086	0.934969	1.100224	0.940087	1.107996	0.942571	1.120057	0.946748	1.124968	0.950717	1.128536	0.956674	1.139304	0.960356	1.148264
Cm244 (at/m3)	0.334017	0.55994	0.394359	0.556193	0.391827	0.557494	0.395466	0.557896	0.39863	0.556571	0.402057	0.5558	0.404639	0.556097	0.40865	0.558263	0.411329	0.561493	0.414026	0.562867
Cm245 (at/m3)	1.244715	1.825557	1.401608	1.814626	1.410418	1.823616	1.420762	1.816513	1.427512	1.811097	1.434117	1.813888	1.435975	1.816734	1.447485	1.819722	1.453386	1.832783	1.460905	1.835931
He4 (at/m3)	0.284558	0.321096	0.28744	0.322343	0.29204	0.312452	0.291118	0.3019	0.282777	0.293455	0.274706	0.291664	0.264996	0.287293	0.258918	0.281214	0.261249	0.274156	0.258742	0.26702

**Table 2.3. (Continued).**

RMSE	41% Pu		43% Pu		45% Pu		47% Pu		49% Pu		51% Pu	
	MOX/SFR UPDATED	MOX/SFR OLD										
	81x16	41x11										
U234 (at/m3)	0.043193	1.848861	0.31058	14.83192	0.30495	13.736	0.299038	17.9653	0.293025	16.77269	0.615987	4.5
U235 (at/m3)	0.079114	0.554011	0.661748	0.955828	0.608528	0.9601	0.567824	0.971293	0.530084	0.975878	0.455756	0.988024
U236 (at/m3)	0.06307	0.113007	0.045449	0.569865	0.063132	0.534197	0.058546	0.566314	0.055775	0.54788	0.052037	0.560448
U237 (at/m3)	0.150761	0.099193	0.234496	0.886866	0.218411	0.880117	0.209984	0.888897	0.198827	0.886536	0.189779	0.888553
U238 (at/m3)	0.012396	0.024184	0.350545	0.359683	0.34884	0.351168	0.338549	0.342809	0.330561	0.334754	0.322825	0.326775
Np237 (at/m3)	0.093569	0.064645	0.186951	0.799431	0.174434	0.784684	0.164485	0.7834	0.156994	0.77144	0.148526	0.762865
Np238 (at/m3)	0.247773	0.206136	0.763844	0.938116	0.753679	0.932744	0.743945	0.931044	0.735156	0.926227	0.725303	0.922291
Np239 (at/m3)	0.115538	0.230778	3.683975	3.863658	3.861305	3.920729	3.919244	4.002392	3.99768	4.083083	0.415	4.161103
U238 (at/m3)	0.033574	0.03786	0.247615	0.249803	0.243651	0.244345	0.238455	0.238965	0.233499	0.233756	0.228647	0.228561
Pu239 (at/m3)	0.042527	0.006087	1.20807	1.22853	1.122052	1.129882	1.02668	1.038091	0.942301	0.952961	0.864473	0.87412
Pu240 (at/m3)	0.009457	0.0084	0.218632	0.199709	0.217429	0.208254	0.224675	0.215093	0.228974	0.220514	0.232211	0.22467
Pu241 (at/m3)	0.004543	0.025609	0.333182	0.352815	0.337942	0.343498	0.326497	0.334716	0.318813	0.326658	0.311629	0.319001
Pu242 (at/m3)	0.014009	0.021027	0.135514	0.139209	0.131517	0.136156	0.128592	0.133039	0.125469	0.130081	0.1224	0.127031
Am241 (at/m3)	0.055148	0.047794	0.011675	0.008385	0.012321	0.011816	0.018715	0.017742	0.024267	0.023322	0.029218	0.028265
Am242 (at/m3)	0.08477	0.076573	0.742065	0.730346	0.73167	0.727432	0.731422	0.724594	0.728667	0.721779	0.725963	0.719082
Am243 (at/m3)	0.090174	0.154778	0.250748	0.23646	0.229604	0.227463	0.226214	0.218894	0.21802	0.211217	0.210563	0.203938
Am242m (at/m3)	0.270244	0.276467	0.663253	0.650026	0.653447	0.648965	0.654486	0.647963	0.653384	0.646784	0.652279	0.645766
Cm242 (at/m3)	0.180328	0.179607	0.744856	0.733309	0.734359	0.730211	0.733711	0.727195	0.730746	0.724165	0.727848	0.721321
Cm243 (at/m3)	0.960292	1.166439	0.548946	0.558303	0.549421	0.555514	0.54988	0.553945	0.548931	0.553374	0.549048	0.554203
Cm244 (at/m3)	0.41558	0.531605	0.60278	0.534871	0.572272	0.519438	0.551831	0.50444	0.529917	0.489272	0.508428	0.475006
Cm245 (at/m3)	1.462319	1.815733	0.715335	0.773916	0.727327	0.782694	0.741379	0.796625	0.756988	0.81423	0.777765	0.832613
He4 (at/m3)	0.250966	0.2565	0.266782	0.205521	0.258188	0.228887	0.256252	0.222701	0.250282	0.219429	0.206589	0.216272

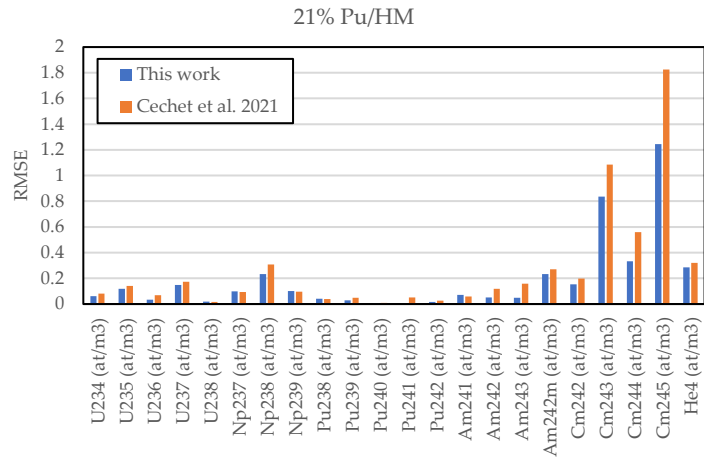


**Fig 2.5.** Comparison of the RMSE values of the two burnup modules for the different nuclides for the SFR case at 21% initial plutonium enrichment.

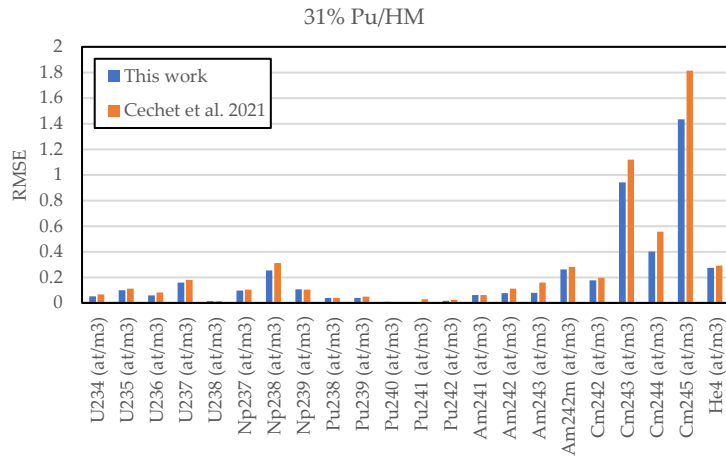


**Fig 2.6.** Comparison of the RMSE values of the two burnup modules for the different nuclides for the SFR case at 31% initial plutonium enrichment.

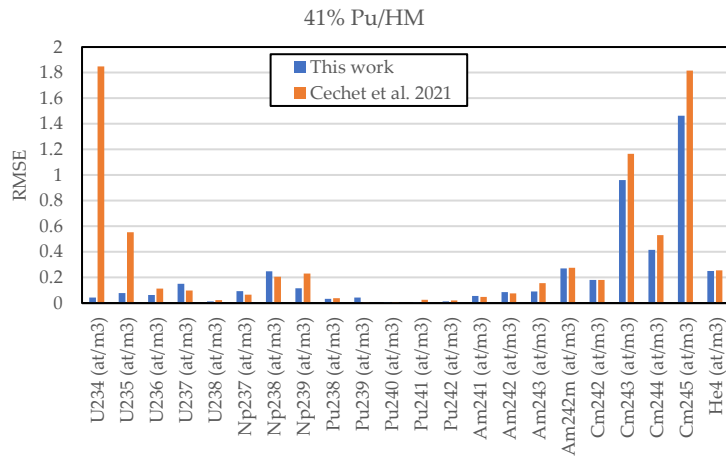


**Fig 2.7.** Comparison of the RMSE values of the two burnup modules for the different nuclides for the SFR case at 41% initial plutonium enrichment.

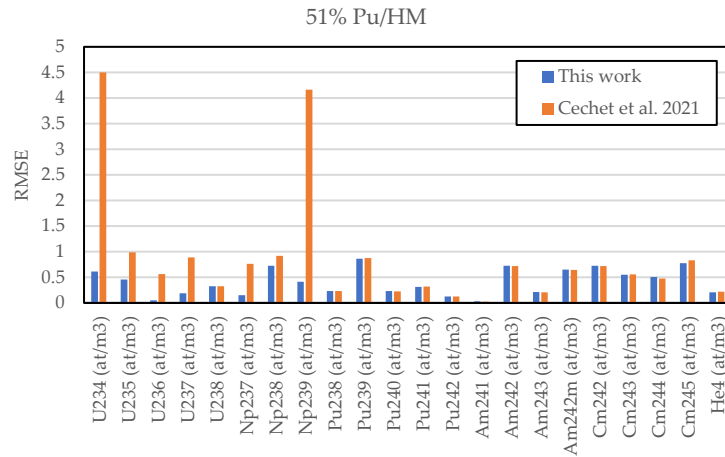


**Fig 2.8.** Comparison of the RMSE values of the two burnup modules for the different nuclides for the SFR case at 51% initial plutonium enrichment.

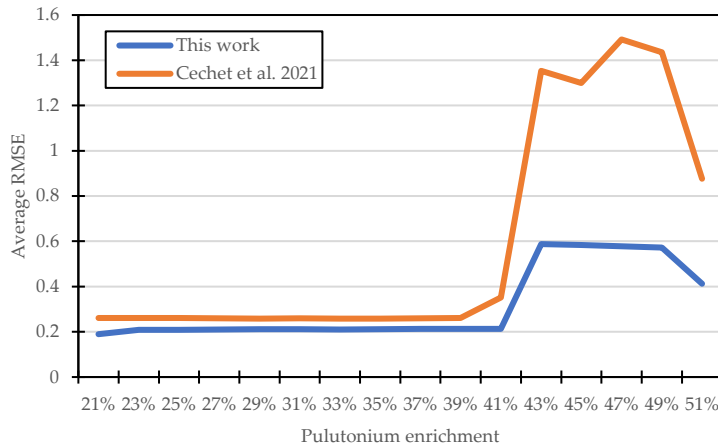


**Fig 2.9.** Evolution of the average RMSE of the two versions of the SCIANTIX burnup module for the SFR case.

Similarly, in Figs. 2.10-2.13, the RMSE for the LBE-FR case is shown. The extended SCIANTIX burnup module has a better predictive performance regarding most of the considered nuclides for all the enrichment cases. Contrary to the SFR case, where the worse predictions regard the curium isotopes, the module has a higher RMSE regarding  $^{237}\text{U}$ ,  $^{237}\text{Np}$  and  $^{238}\text{Np}$  for all the enrichment cases. Error introduced in the calculation of  $^{237}\text{U}$  production is propagated through to the  $^{237}\text{Np}$  concentration through due to  $\beta$ -decay. For enrichment higher than 40% which is the limit of the definition point of the lookup table for the existing burnup module, the RMSE of  $^{234}\text{U}$  increases sharply, with the module significantly overpredicting the concentration by up to 2 orders of magnitude, resulting to an RMSE of 36.69 which is not reported in Fig. 3.9. In Fig. 2.14 the evolution of the mean RMSE for the two models validate the fact that the model calculations diverge for values of enrichment that are out of bounds of the defined lookup table, which is further attributed to increased burnup for the same irradiation time and fission rate density as increased initial fissile material is introduced in the fuel. In Table 2.4., the RMSE values of all nuclides for each enrichment level for the LBE-FR case are collected.

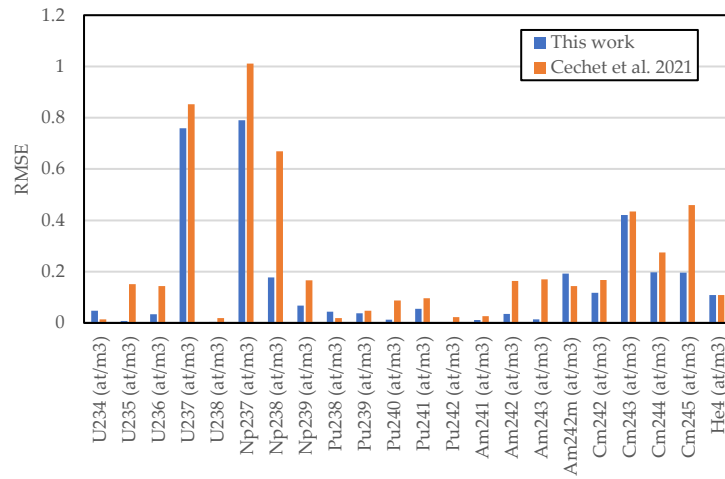


**Fig 2.10.** Comparison of the RMSE values of the two burnup modules for the different nuclides for the LBE-FR case at 21% initial plutonium enrichment.

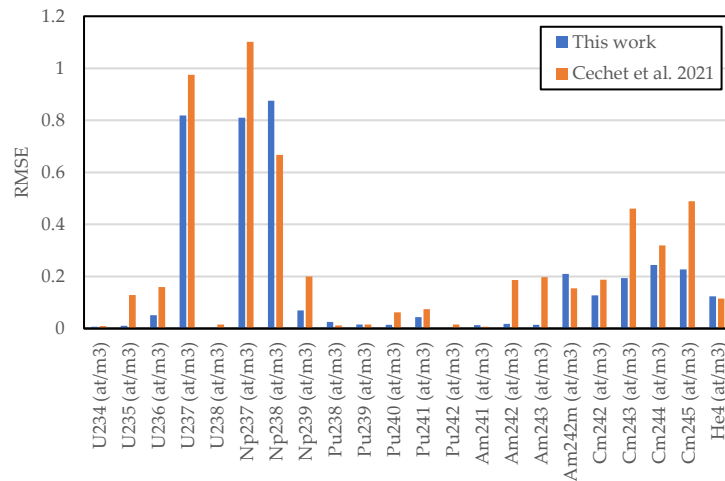


**Fig 2.11.** Comparison of the RMSE values of the two burnup modules for the different nuclides for the LBE-FR case at 31% initial plutonium enrichment.

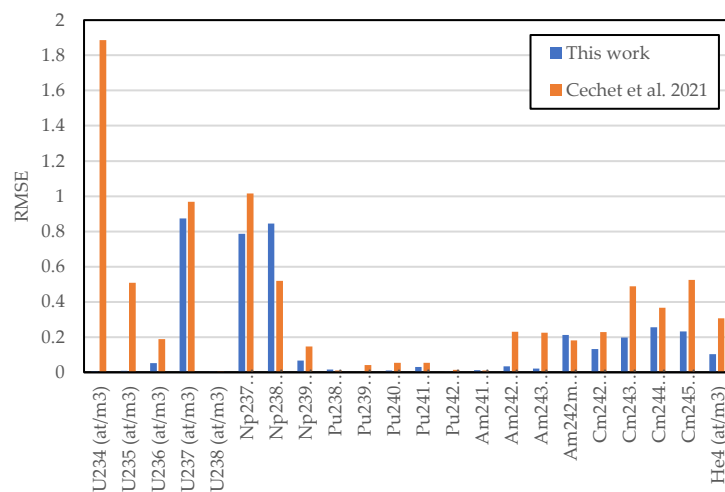


**Fig 2.12.** Comparison of the RMSE values of the two burnup modules for the different nuclides for the LBE-FR case at 41% initial plutonium enrichment.

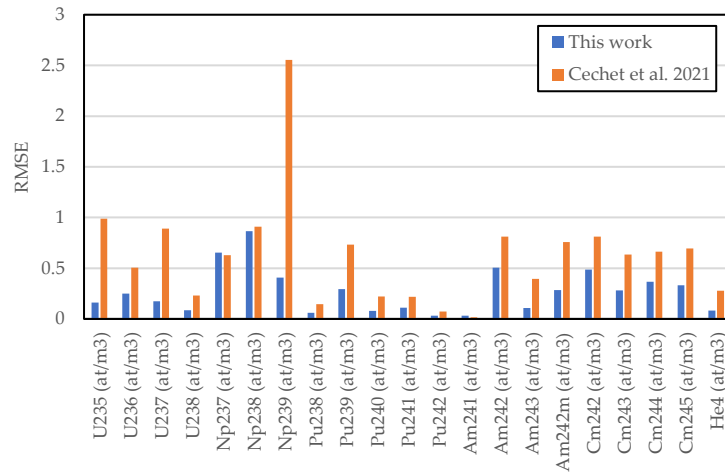


**Fig 2.13.** Comparison of the RMSE values of the two burnup modules for the different nuclides for the LBE-FR case at 51% initial plutonium enrichment.

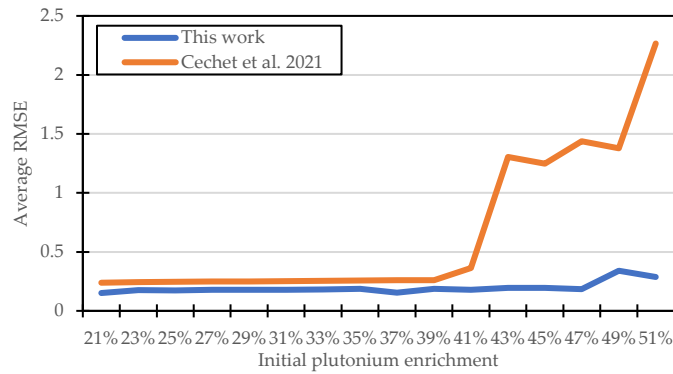


**Fig 2.14.** Evolution of the RMSE of the two versions of the SCIANTIX burnup module for the LBE-FR case.

**Table 2.4.** RMSE values for all the plutonium enrichment steps for all nuclides in the LBE-FE case.

RMSE	21% Pu		23% Pu		25% Pu		27% Pu		29% Pu		31% Pu		33% Pu		35% Pu		37% Pu		39% Pu	
	MOX/LBE_FR_UPDATED	MOX/LBE_FR_OLD																		
U234 (at/m3)	0.04755	0.01352	0.008483	0.0125	0.00784	0.01149	0.00753	0.0105208	0.0073	0.00959	0.007077	0.008654	0.006929	0.00773	0.006748	0.006857	0.006602	0.006007	0.0065032	0.005175
U235 (at/m3)	0.0076	0.15057	0.007177	0.1471	0.00865	0.14294	0.00963	0.138515	0.01006	0.13374	0.010085	0.128639	0.010043	0.12367	0.009804	0.118508	0.009387	0.11333	0.008909	0.108276
U236 (at/m3)	0.03398	0.14387	0.046266	0.1478	0.04829	0.15106	0.04923	0.152765	0.05047	0.15688	0.051229	0.159126	0.052232	0.16076	0.052416	0.162065	0.052499	0.162785	0.0527334	0.163008
U237 (at/m3)	0.75878	0.85233	0.768189	0.8796	0.77319	0.89788	0.78633	0.931969	0.80038	0.94689	0.818499	0.974617	0.820845	0.99608	0.847602	1.026767	0.248196	1.040669	0.8709584	1.063729
U238 (at/m3)	0.00336	0.01851	0.002684	0.0181	0.00215	0.01754	0.00163	0.0169719	0.00118	0.01635	0.000877	0.015695	0.000888	0.01504	0.001115	0.014369	0.001465	0.013685	0.0018381	0.013016
Np237 (at/m3)	0.79008	1.01134	0.781696	1.0389	0.79166	1.05508	0.79016	1.0843013	0.80558	1.08939	0.810265	1.10186	0.797552	1.10086	0.809562	1.118687	0.804182	1.117063	0.7992683	1.104472
Np238 (at/m3)	0.17703	0.66953	0.878645	0.6747	0.86913	0.67207	0.86135	0.6806703	0.87307	0.67044	0.874712	0.667348	0.859168	0.65442	0.869627	0.657266	0.863272	0.646308	0.8580431	0.626627
Np239 (at/m3)	0.06808	0.1661	0.0677	0.1737	0.0687	0.18087	0.06921	0.1877062	0.06955	0.19423	0.069547	0.200228	0.069471	0.20599	0.069272	0.21137	0.068657	0.216155	0.0679752	0.220926
Pu238 (at/m3)	0.04341	0.01937	0.03839	0.0176	0.034	0.01599	0.03049	0.0145724	0.02744	0.0133	0.024823	0.012207	0.022285	0.01123	0.020282	0.010476	0.01843	0.009886	0.0167349	0.009435
Pu239 (at/m3)	0.03803	0.04774	0.035853	0.0408	0.02889	0.03399	0.02376	0.027433	0.01925	0.02112	0.015141	0.015211	0.011488	0.00973	0.008425	0.004897	0.005722	0.002384	0.0034856	0.005149
Pu240 (at/m3)	0.01199	0.08696	0.016487	0.0809	0.01476	0.07538	0.01441	0.0705789	0.01418	0.06627	0.013872	0.0624	0.013284	0.05911	0.012712	0.056126	0.012124	0.053445	0.0115934	0.051072
Pu241 (at/m3)	0.05481	0.09599	0.063965	0.0907	0.05502	0.08589	0.05066	0.0816701	0.04683	0.07781	0.043377	0.074253	0.04037	0.07109	0.037552	0.068129	0.035074	0.065346	0.0328271	0.062764
Pu242 (at/m3)	0.00173	0.02301	0.001809	0.0211	0.00092	0.0194	0.00059	0.0179912	0.00094	0.01682	0.001447	0.015831	0.001947	0.01501	0.002402	0.014341	0.002792	0.013784	0.0031547	0.013348
Am241 (at/m3)	0.01183	0.02685	0.015942	0.0208	0.0148	0.01574	0.01414	0.0118127	0.01362	0.00888	0.013124	0.007133	0.01279	0.00639	0.0124	0.006426	0.012096	0.006805	0.0118639	0.00726
Am242 (at/m3)	0.03453	0.16423	0.035372	0.1683	0.0232	0.17255	0.01831	0.1770856	0.01625	0.18182	0.017481	0.186482	0.020334	0.19122	0.023977	0.195824	0.027505	0.200158	0.0310777	0.204509
Am243 (at/m3)	0.01428	0.17013	0.009176	0.1761	0.00992	0.18146	0.01138	0.1871234	0.01284	0.19248	0.014322	0.19759	0.015776	0.20268	0.017535	0.207457	0.018603	0.212104	0.0201572	0.216517
Am242m (at/m3)	0.19247	0.14312	0.211412	0.1449	0.20924	0.14708	0.20925	0.1495605	0.20959	0.15225	0.209738	0.154941	0.210432	0.15816	0.211019	0.161258	0.211163	0.164275	0.211609	0.167245
Cm242 (at/m3)	0.11748	0.16762	0.126974	0.1713	0.12576	0.17528	0.12583	0.1794515	0.12638	0.18373	0.12696	0.187887	0.128151	0.19231	0.129427	0.196438	0.130289	0.200399	0.1313072	0.204237
Cm243 (at/m3)	0.42068	0.43498	0.193548	0.4404	0.19407	0.44617	0.27443	0.451132	0.19491	0.45665	0.194333	0.460578	0.276662	0.46639	0.27751	0.470951	0.277489	0.475045	0.2779115	0.478376
Cm244 (at/m3)	0.19745	0.27469	0.238303	0.2849	0.23691	0.29403	0.23894	0.303211	0.24188	0.31174	0.243783	0.319611	0.24678	0.32747	0.250314	0.334683	0.25162	0.341468	0.2541246	0.34789
Cm245 (at/m3)	0.19628	0.45899	0.224473	0.4663	0.22327	0.47318	0.22466	0.4791041	0.31989	0.48489	0.226536	0.489359	0.227692	0.4951	0.325463	0.499928	0.229909	0.503537	0.3270017	0.507121
He4 (at/m3)	0.10882	0.10925	0.104165	0.1403	0.10109	0.13442	0.09682	0.1297053	0.09204	0.12053	0.123827	0.114669	0.1178	0.1107	0.112992	0.105187	0.111035	0.156512	0.1073096	0.151112

**Table 2.4. (Continued).**

RMSE	41% Pu		43% Pu		45% Pu		47% Pu		49% Pu		51% Pu	
	MOX/LB E_FR	MOX/LB E_FR	MOX/LBE _FR	MOX/L BE_FR	MOX/LB E_FR	MOX/LB E_FR	MOX/LB E_FR	MOX/LBE FR	MOX/LB E_FR	MOX/LB E_FR	MOX/LBE _FR	MOX/LBE FR
U234 (at/m3)	0.00639	1.8855	0.00632	15.201	0.00627	14.0427	0.00617	18.297862	0.07353	17.0589	0.692935	36.69458
U235 (at/m3)	0.00842	0.50907	0.00788	0.9563	0.00743	0.9591	0.00697	0.9716007	0.07907	0.97586	0.161912	0.988024
U236 (at/m3)	0.05253	0.1877	0.052224	0.5558	0.05166	0.5012	0.05095	0.5211538	0.05267	0.49987	0.248198	0.503809
U237 (at/m3)	0.87306	0.96801	0.890555	0.8974	0.8974	0.88842	0.91639	0.891777	0.78086	0.8893	0.173699	0.889122
U238 (at/m3)	0.0022	0.00377	0.00254	0.255	0.00282	0.24893	0.00311	0.2429631	0.10767	0.23722	0.086513	0.2316
Np237 (at/m3)	0.78628	1.01513	0.771949	0.6989	0.75957	0.67546	0.75777	0.6623519	0.61205	0.64416	0.654365	0.628177
Np238 (at/m3)	0.8453	0.51949	0.830854	0.9301	0.81954	0.92389	0.81901	0.9196926	0.77541	0.91428	0.86678	0.909186
Np239 (at/m3)	0.06711	0.14657	0.066331	2.3396	0.06551	2.396	0.06481	2.4506266	1.77856	2.50323	0.408636	2.554347
Pu238 (at/m3)	0.0152	0.00947	0.013838	0.1514	0.01257	0.14968	0.01149	0.147846	0.05751	0.14605	0.060001	0.144139
Pu239 (at/m3)	0.00163	0.04022	0.000648	1.0096	0.00138	0.93242	0.00228	0.8604289	0.33269	0.79348	0.292885	0.731449
Pu240 (at/m3)	0.01097	0.05313	0.010387	0.2236	0.00974	0.22432	0.00921	0.2242744	0.06975	0.22376	0.077976	0.222698
Pu241 (at/m3)	0.03069	0.0537	0.02887	0.2379	0.02713	0.23293	0.02548	0.2280893	0.14025	0.22335	0.110069	0.218653
Pu242 (at/m3)	0.00347	0.01315	0.003784	0.0778	0.00405	0.0765	0.00431	0.0751628	0.03357	0.07386	0.033233	0.072553
Am241 (at/m3)	0.01171	0.01092	0.011586	0.0421	0.01151	0.03415	0.0115	0.0269834	0.02486	0.02057	0.032534	0.014782
Am242 (at/m3)	0.03432	0.23005	0.037243	0.8166	0.03998	0.81524	0.04223	0.8139539	0.50404	0.81272	0.504628	0.811528
Am243 (at/m3)	0.02152	0.22531	0.022922	0.4234	0.02466	0.41612	0.02584	0.4089421	0.10469	0.402	0.106877	0.395538
Am242m (at/m3)	0.21197	0.18027	0.211955	0.7572	0.2131	0.75771	0.21311	0.7581656	0.27753	0.75857	0.285098	0.759045
Cm242 (at/m3)	0.13231	0.22859	0.132821	0.8166	0.13461	0.81506	0.13523	0.8136244	0.48531	0.81224	0.486848	0.810954
Cm243 (at/m3)	0.19651	0.48819	0.277563	0.6605	0.28	0.65388	0.27904	0.6475081	0.25345	0.64113	0.280503	0.634986
Cm244 (at/m3)	0.25624	0.36646	0.257334	0.7059	0.262	0.69555	0.26257	0.685154	0.34548	0.6746	0.367567	0.664418
Cm245 (at/m3)	0.23167	0.52501	0.326857	0.7299	0.33117	0.7209	0.33041	0.7120635	0.28321	0.703	0.331809	0.69473
He4 (at/m3)	0.10301	0.30626	0.342351	0.2309	0.32957	0.30084	0.09433	0.2921392	0.311	0.28738	0.083506	0.277548

Regarding the evolution of the concentration of selected nuclides calculated by the extended burnup module, a comparison with the SERPENT calculated concentrations is shown in Fig. 2.15-3.28 for the 31% enrichment level. The nuclides shown correspond to those incorporated in the helium correlation in Section 2.5, as well as those with higher RMSE. The profiles confirm a satisfactory agreement for all nuclides for both test cases and in line with the performance of other fuel burnup models like TUBRNP [36]. Additionally, a better agreement between the burnup module and the SERPENT depletion results is observed for nuclides initially present in the fuel as reported by Cechet et al. 2021 [18].

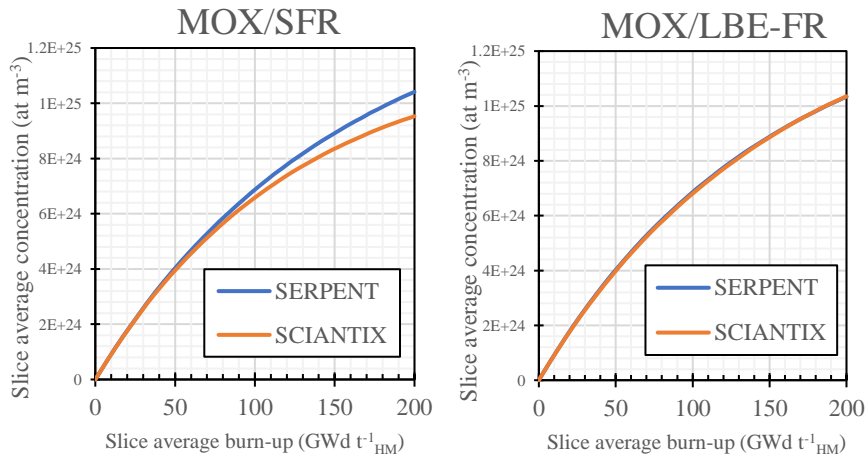


**Fig 2.15.** Evolution of the <sup>234</sup>U concentration for the two fuel/reactor cases at 31% Pu/HM enrichment.

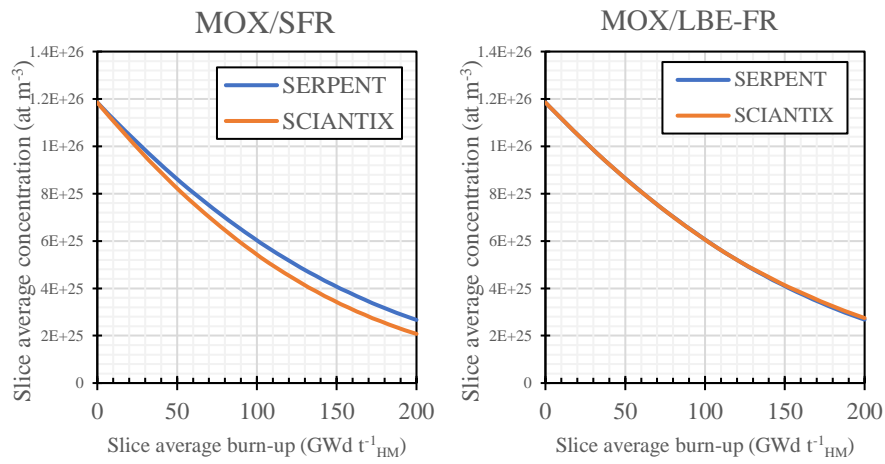


**Fig 2.16.** Evolution of the  $^{235}\text{U}$  concentration for the two fuel/reactor cases at 31% Pu/HM enrichment.

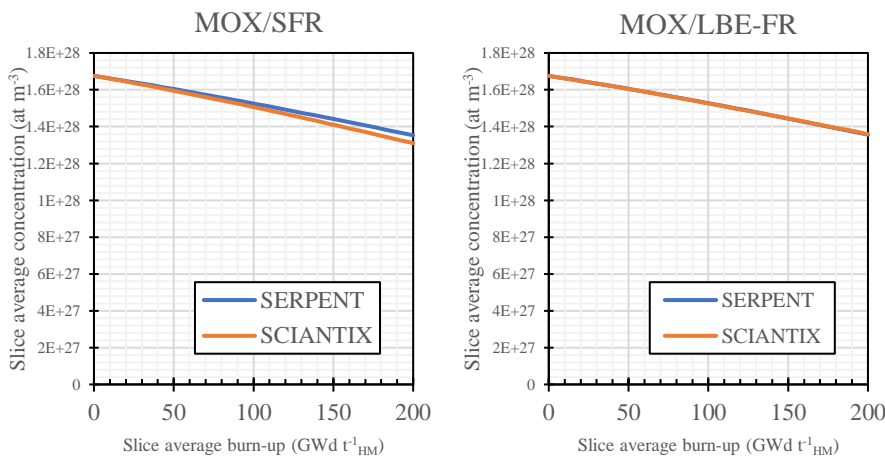


**Fig 2.17.** Evolution of the  $^{238}\text{U}$  concentration for the two fuel/reactor cases at 31% Pu/HM enrichment.

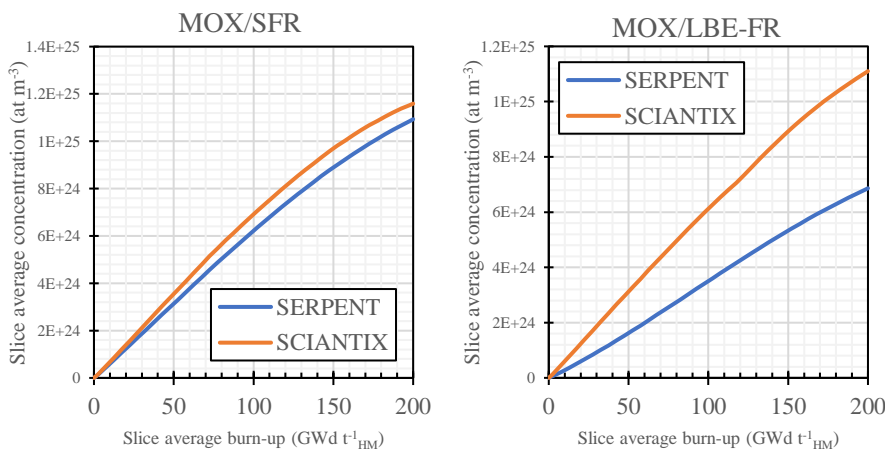


**Fig 2.18.** Evolution of the  $^{237}\text{Np}$  concentration for the two fuel/reactor cases at 31% Pu/HM enrichment.

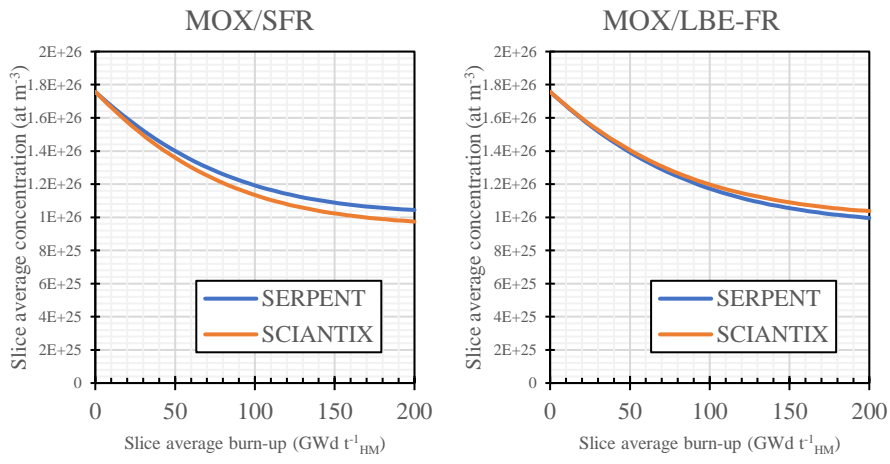


Fig 2.19. Evolution of the  $^{238}\text{Pu}$  concentration for the two fuel/reactor cases at 31% Pu/HM enrichment.

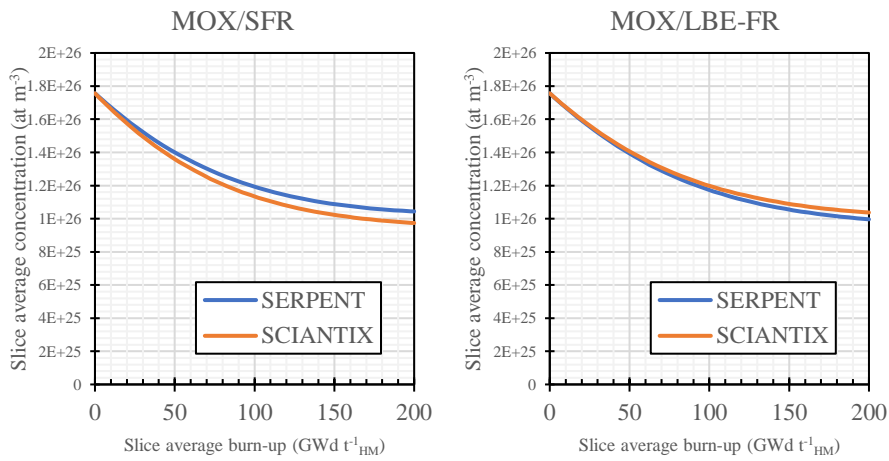


Fig 2.20. Evolution of the  $^{239}\text{Pu}$  concentration for the two fuel/reactor cases at 31% Pu/HM enrichment.

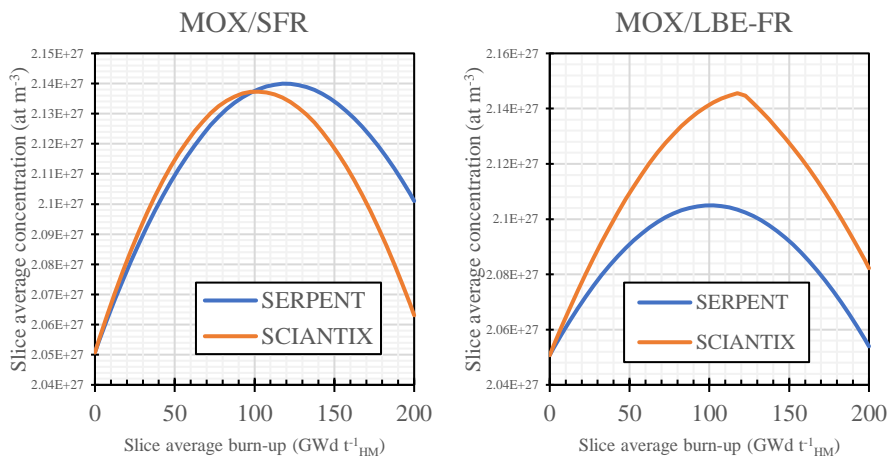


Fig 2.21. Evolution of the  $^{240}\text{Pu}$  concentration for the two fuel/reactor cases at 31% Pu/HM enrichment.

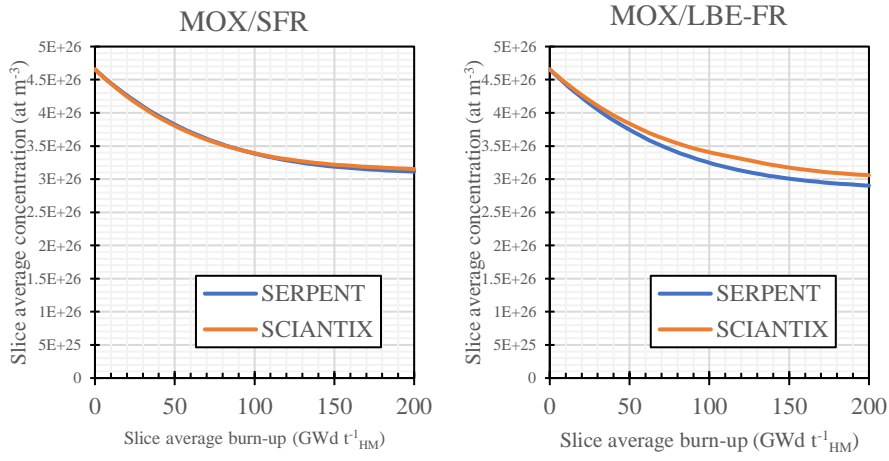


Fig 2.22. Evolution of the  $^{241}\text{Pu}$  concentration for the two fuel/reactor cases at 31% Pu/HM enrichment.

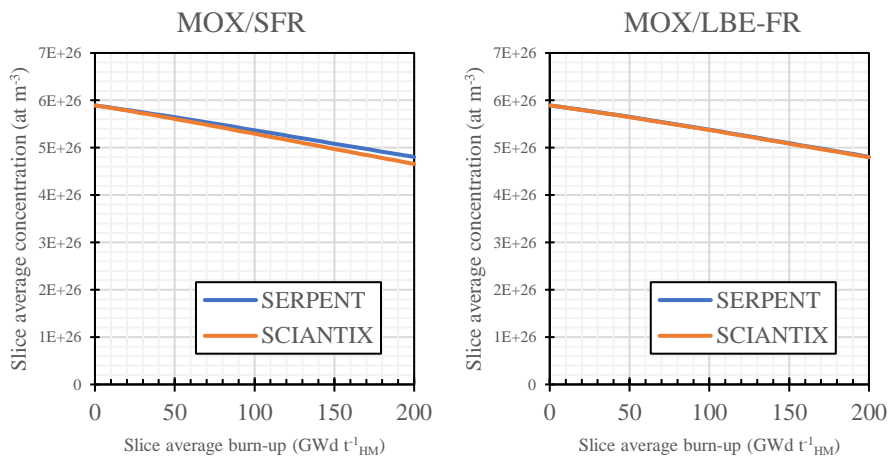


Fig 2.23. Evolution of the  $^{242}\text{Pu}$  concentration for the two fuel/reactor cases at 31% Pu/HM enrichment.

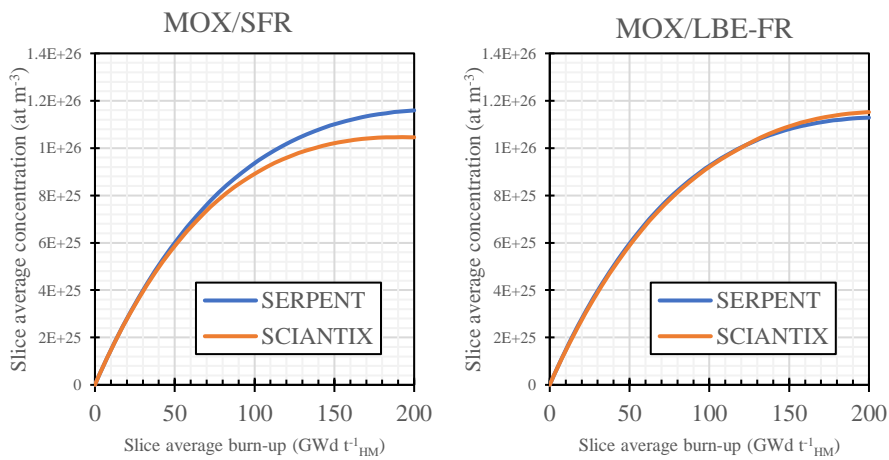


Fig 2.24. Evolution of the  $^{241}\text{Am}$  concentration for the two fuel/reactor cases at 31% Pu/HM enrichment.

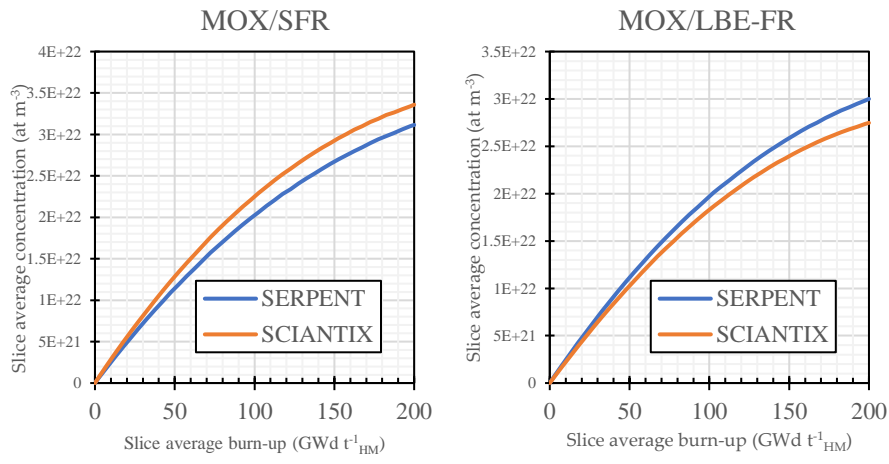


Fig 2.25. Evolution of the  $^{242}\text{Am}$  concentration for the two fuel/reactor cases at 31% Pu/HM enrichment.

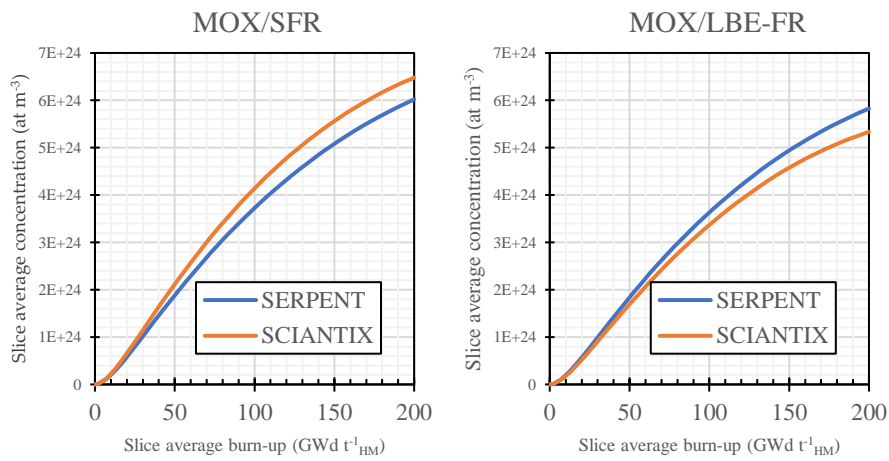


Fig 2.26. Evolution of the  $^{242}\text{Cm}$  concentration for the two fuel/reactor cases at 31% Pu/HM enrichment.

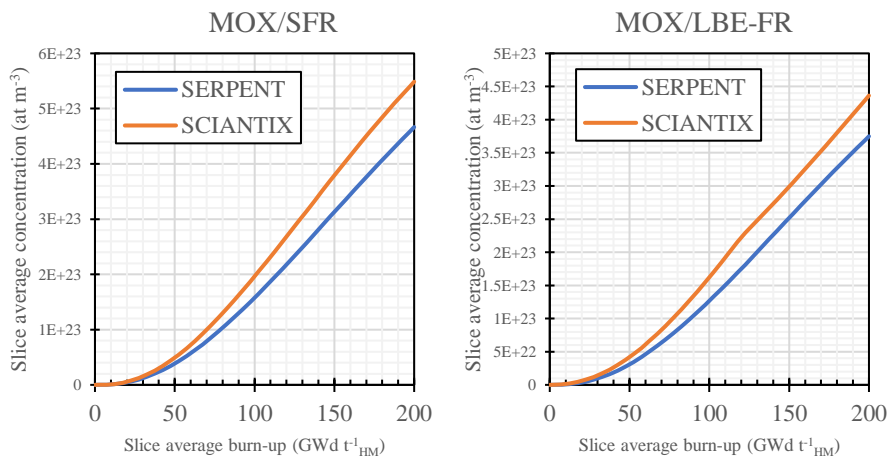
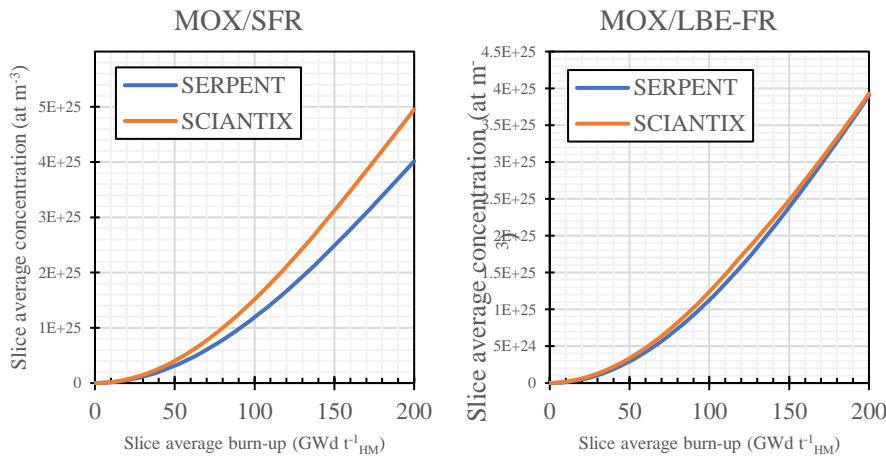


Fig 2.27. Evolution of the  $^{243}\text{Cm}$  concentration for the two fuel/reactor cases at 31% Pu/HM enrichment.



**Fig 2.28.** Evolution of the  $^{244}\text{Cm}$  concentration for the two fuel/reactor cases at 31% Pu/HM enrichment.

In addition to the verification with the SERPENT high-fidelity results, the extended burnup module is validated against experimental data from the SUPERFACT-1 and SPHERE irradiation experiments [4,5]. The specifications of each case are shown in Table 2.5. The validation is performed based on End of Life (EoL) concentrations of selected nuclides. Regarding the SUPERFACT-1 experimental data, for the SF13 fuel pin, a comparison between  $^{237}\text{Np}$  concentration and total plutonium content at the EoL fuel conditions with the SCIANTIX burnup module calculated concentrations is performed. For the SF16 fuel pin, a comparison between total plutonium content and  $^{241}\text{Am}$  concentration at the EoL fuel condition with the calculated values. The results are shown in Table 2.6. The burnup module exhibits good predictive performance for the calculated nuclides consistent with the trend of the RMSE exhibited in the verification results. Regarding the SPHERE experimental data, the EoL concentrations of 31 nuclides are available, which are also tracked by the SCIANTIX burnup module, which enables a more in-depth validation with multiple nuclides of the same decay chain. The results are shown in Fig 2.29. The model performs well for most of the nuclides with exceptions for  $^{239}\text{Np}$ ,  $^{244}\text{Am}$  and  $^{240}\text{Pu}$  which has a relative error of 5110% and is not shown in the figure. The total average error for the SPHERE irradiation experiment is 0.8442 which is significantly affected by the aforementioned nuclides. The observed discrepancies are ascribed to the peculiar neutron spectrum of the SPHERE experiment, which was designed to test a fuel pin for fast reactors but was irradiated in a light water reactor with a wrapper absorbing thermal neutrons.

**Table 2.5.** Specifications for the simulations of the two irradiation experiments used for preliminary validation of the SCIANTIX burnup module.

Parameter	SUPERFACT-1		SPHERE
	SF13 fuel pin	SF16 fuel pin	Fuel pin
Pellet radius (mm)	2.68	2.71	2.825
Pellet density (%TD)	97.5	96.3	93.8
Fuel pin length (mm)	850	850	58.915
U/HM (%)	74.1 <sup>a</sup>	74.5 <sup>a</sup>	76 <sup>b</sup>
MA/HM	2%, <sup>237</sup> Np	1.8%, <sup>241</sup> Am	3%, <sup>241</sup> Am
Pu/HM (%)	24.4 <sup>c</sup>	23.7 <sup>c</sup>	20 <sup>d</sup>
O/M (\)	1.943	1.957	1.952
Irradiation time (h)	10880	10880	14576
Burnup (at EoL) (GWd/tHM)	62.05	61.53	44.064

<sup>a</sup>Natural uranium composition.

<sup>b</sup> $^{234}\text{U}$  0.03092%,  $^{235}\text{U}$  0.2878%,  $^{236}\text{U}$  0.018%,  $^{238}\text{U}$  99.66%

<sup>c</sup> $^{238}\text{Pu}$  1.3%,  $^{239}\text{Pu}$  60.4%,  $^{240}\text{Pu}$  23.4%,  $^{241}\text{Pu}$  10.4%,  $^{242}\text{Pu}$  4.5%

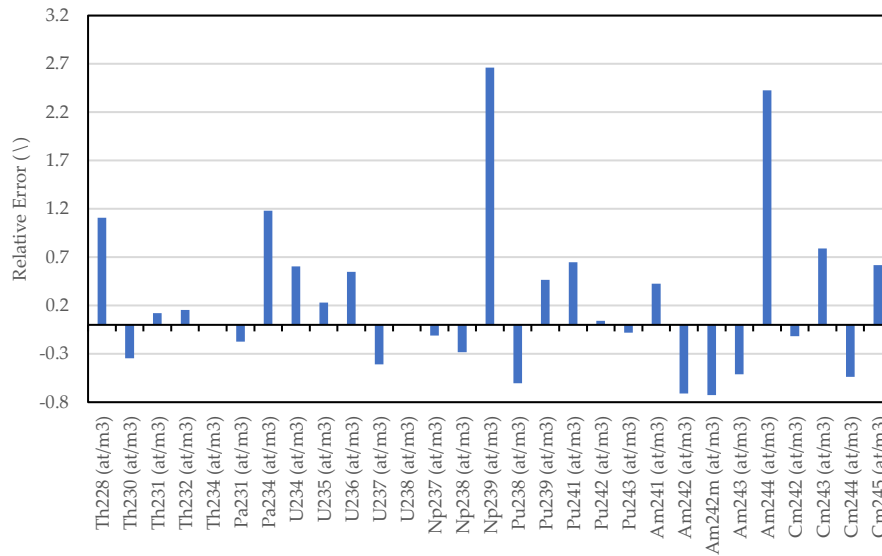
<sup>d</sup> $^{238}\text{Pu}$  0.017%,  $^{239}\text{Pu}$  90.63%,  $^{240}\text{Pu}$  9.16%,  $^{241}\text{Pu}$  0.1236%,  $^{242}\text{Pu}$  0.07363%

**Table 2.6.** Validation of the SCIANTIX burnup module with the SUPERFACT-1 results.

SF13			
	Predicted	Experimental	Relative error (%)
Total Np	$3.33 \cdot 10^{26}$	$3.2747 \cdot 10^{26}$	1.562739023
Total Pu	$5.54 \cdot 10^{27}$	$5.35935 \cdot 10^{27}$	3.350390472

SF16			
	Predicted	Experimental	Relative error (%)
Total Pu	$5.57 \cdot 10^{27}$	$5.24749 \cdot 10^{27}$	6.211150229
<sup>241</sup> Am	$3.20 \cdot 10^{26}$	$3.69469 \cdot 10^{27}$	-13.49311024



**Fig 2.29.** Relative error for each nuclide calculated by the SCIANTIX burnup module for the SPHERE irradiation experiment.

## 2.4 Development of a surrogate model for helium production

In this section the methodology of the development of a surrogate model to calculate helium production in nuclear fuel is presented, with focus on the Latin hypercube sampling (LHS) method employed. The basic tool employed is the hereabove presented, extended SCIANTIX burnup module since it is fast running, and adequately accurate for the prediction of helium production in nuclear fuel. The burnup module is used to populate several synthetic datasets with calculated helium concentration values as a function of the input variable matrix. The output vector  $Y_{N,n} = h(X_{i,n})$  (i.e., the helium concentration) is calculated by the code as a function of a selection of  $n$  values of  $N$  input variables  $X_{i,n} = (X_{1,n}, X_{2,n}, \dots, X_{N,n})$ , sampled from predefined. By examining the probability distribution of the output  $Y_{N,n}(X)$  the desired information of the dependence of helium concentration on each input variable can be obtained. Consequently, the output  $Y_{N,n}$  can be correlated to an unknown transformation  $h(X_{i,n})$  of the inputs  $X_{i,n}$  which have a known probability distribution  $F(x)$  for  $x \in S$  where  $S$  is the sample space of  $X_i$ . Several values of  $X$  ( $X_1, X_2, \dots, X_N$ ) must be selected as successive inputs sets to obtain the desired information on the output  $Y_{N,n}$ . The number of input variables  $N$  and the number of values sampled  $n$  dictate the computational time for the development of the synthetic datasets (e.g., for the generation of a 10000 values dataset, using 1000 integration points in the SCIANTIX burnup module, the computational time required is around 3.15 hours).

To ensure that each of the input variables  $X_{i,n}$  has all portions of its distribution represented by input values, the range of each  $X_{i,n}$  is divided into  $M$  strata of equal marginal probability  $1/M$  and sampled only once from each stratum [37]. Using this technique, the advantage of limiting the amount of input values per each input variable and represent them in a fully stratified manner is evident, without a biased projection of the values that end up being important in the final statistical model. For this reason, this type of sampling is widely employed in the field of Generation IV nuclear reactors' design as well as in the field of risk assessment of nuclear power stations [38-40]. For example, Fig. 2.30 reports the Pu/HM input variable distribution is shown for 881 data points, highlighting the dense coverage of values over the sampling space without specific point concentration that would introduce bias to the analysis. The computational times using this "memory"-specific approach are significantly decreased relatively to other processes of multidimensional random sampling like Monte-Carlo sampling, for the same order of relative error achieved [41].

The input variables considered in this analysis were the fuel initial composition in terms of all constituent nuclides expressed as the ratio of each nuclide per heavy metal ( $iX/HM$ ), the initial oxygen to metal ratio of the fuel O/M, the initial fuel density  $\rho_{fuel}$ , the fuel temperature  $T_{fuel}$ , the irradiation time  $t_{irr}$  and the fission rate density  $\dot{F}$ . The ranges of each variable limits are shown in Table 2.7. The limits are chosen in-line with the predictive capabilities of the extended SCIANTIX burnup module as well as for the fuel specifications of a selection of Generation IV reactors core concepts [42]. The implementation of the LHS method is performed in MATLAB [43] coupled with the SCIANTIX code for the helium concentration calculation. The training dataset is composed of the multidimensional input matrix  $X_{i,n}$  representing the contribution of each input variable, and an output vector  $Y_{N,n}$  representing the helium concentration. Subsequently, multivariate non-linear regression and statistical analysis was performed with the JMP statistical package [44] to formulate a surrogate model for the two reactor cases of interest, SFR and LBE-FR. The method of stepwise regression employed is forward regression.

The input vectors corresponding to the irradiation time  $t_{irr}$  and the helium concentration are linearized as preliminary single regression analysis exhibited a non-linear trend between them (plotting of the residuals versus the two regressors) by considering the respective logarithmic quantities. The dependence of the plutonium content is considered by using a 3<sup>rd</sup> degree polynomial term as the residuals plot exhibited this trend. The rest of the input variables were added in a linear fashion in the correlation (see Eq. 2.10).

The regression is performed by considering the p-values of each regressor with respect to the output values in an iterative process, in which each regressor is added to the formulation only if its respective p-value is below the 0.05 threshold. Within this approach, collinearity between input variables is avoided by including only one of the inter-correlated variables in the final model (e.g., irradiation time is heavily correlated with burnup, so only the irradiation time is considered in the final model). At each iteration step, after a variable has been added to the model, the p-values change accordingly for each variable. This iterative process considers the importance of the order in which the model is progressively built, as it heavily affects the weights of each variable at each iteration step.

With this procedure and considering the afore-mentioned requirements and restrictions, 2 surrogate models were chosen out of  $11 \cdot 10^6$  examined candidates. The proposed surrogate models for both the SFR, and the LBE-FR case comprise of seven dependencies which are the irradiation time  $t_{irr}$ , the fission rate density  $\dot{F}$ , the total plutonium content Pu/HM, the fuel density  $\rho_{fuel}$ , the initial americium-241 concentration  $^{241}\text{Am}/\text{HM}$ , the initial americium-242 concentration  $^{242}\text{Am}/\text{HM}$ , and the initial curium-242 concentration  $^{242}\text{Cm}/\text{HM}$ . The quality of the final fit and the accuracy of the models were quantified in terms of the RMSE (as defined in Section 2.2), the coefficient of determination  $R^2$  and the adjusted coefficient of determination  $R^2_{adj}$  [45]. The  $R^2_{adj}$  metric provides information on the artificial increase of the  $R^2$  value when adding more contributions to the predictive model and must approach the value of  $R^2$  to ensure a non-overfitted model. The proposed models and the statistical metrics for each case are reported in the next section.

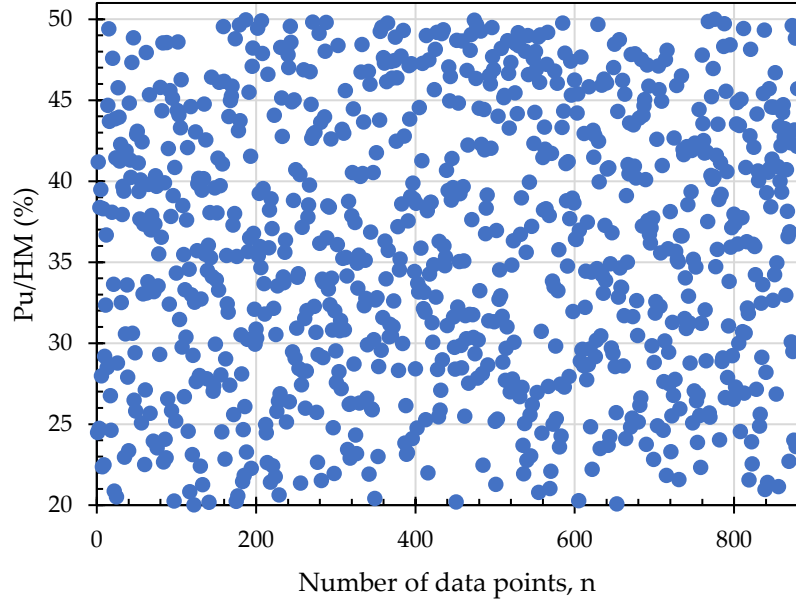


**Fig. 2.30.** Scatterplot produced using the LHS method for 881 data points of Pu/HM values as an example of an input variable bias-less coverage density.

## 2.5 Validation of the helium production surrogate models

The ranges of the considered input variables are shown in Table 2.7. The limits of the variable ranges were chosen with both the definition grid of the SCIANTIX extended burnup module and the needs and prospects of Generation IV reactor fuel research in mind, as well as existing reports of experimental data on MA-containing MOX fuel [47-51]. Regarding the individual isotopes of each element, the limits follow the same range as the total value per heavy metal, so they are not reported in the table (e.g.,  $^{241}\text{Am}/\text{HM}$  has values ranging from 0 to 5% as is the total americium per heavy metal). The proposed surrogate models for the SFR and the LBE-FR cases are in the form of:

$$\begin{aligned}
 \log[^4\text{He}] = & A \cdot \log [t_{\text{irr}}] \\
 & + B \cdot \dot{F} \\
 & + (C \cdot [\text{Pu}] + D \cdot [\text{Pu}]^2 + E \cdot [\text{Pu}]^3) \\
 & + F \cdot \rho_{\text{fuel}} \\
 & + G \cdot [^{241}\text{Am}] + H \cdot [^{242}\text{Am}] \\
 & + I \cdot [^{242}\text{Cm}] \\
 & + S
 \end{aligned} \tag{2.10}$$

where  $t_{\text{irr}}$  is the irradiation time (h),  $\dot{F}$  is the fission rate density ( $\text{fiss m}^{-3} \text{s}^{-1}$ ),  $[\text{Pu}]$  is the total plutonium over heavy metal ratio (%),  $\rho_{\text{fuel}}$  is the fuel density ( $\text{kg m}^{-3}$ ),  $[^{241}\text{Am}]$  is the americium-241 per heavy metal ratio (%),  $[^{242}\text{Am}]$  is the americium-242 per heavy metal ratio (%),  $[^{242}\text{Cm}]$  is the curium-242 per heavy metal ratio (%) and  $A, B, C, D, E, F, G, H, I$  and  $S$  are coefficients shown in Table 2.8 for the two fuel/reactor combination cases along with the respective standard error of estimation.

**Table 2.7.** Ranges of the input variable values considered for the development of the helium production correlation.

Variable	Symbol	Limit range
Irradiation time (h)	$t_{irr}$	100 - 100000
O/M (\)	O/M	1.95 - 2
Fission rate density (fiss m <sup>-3</sup> s <sup>-1</sup> )	$\dot{F}$	1 10 <sup>18</sup> - 1·10 <sup>19</sup>
<sup>235</sup> U enrichment (%)	[ <sup>235</sup> U]	0.711 - 5
Pu/HM (%)	[Pu]	20 - 50
Np/HM (%)	[Np]	0 - 5
Am/HM (%)	[Am]	0 - 5
Cm/HM (%)	[Cm]	0- 5
Fuel density (kg m <sup>-3</sup> )	$\rho_{fuel}$	9325 - 10970
Fuel Temperature (K)	$T_{fuel}$	900 - 1900

**Table 2.8.** Values of the coefficients in the helium correlation for the two fuel/reactor combinations, with the corresponding standard error.

Coefficient	Variable	SFR	Std. Error	LBE-FR	Std. Error
A	log[ $t_{irr}$ ]	0.669835228	0.00383517	0.6771483301	0.00375305
B	$\dot{F}$	2.58123·10 <sup>-21</sup>	6.0452·10 <sup>-23</sup>	2.6631·10 <sup>-21</sup>	5.8679·10 <sup>-23</sup>
C	[Pu]	-0.90146171	0.01363592	-0.92536684	0.01313788
D	[Pu] <sup>2</sup>	0.0237788448	0.00039144	0.0243855707	0.0003769
E	[Pu] <sup>3</sup>	-0.000204616	3.64727·10 <sup>-6</sup>	-0.000209562	3.50935·10 <sup>-6</sup>
F	$\rho_{fuel}$	0.0000311663	3.48953·10 <sup>-6</sup>	0.000037483	3.38246·10 <sup>-6</sup>
G	[ <sup>241</sup> Am]	0.0680062668	0.00398778	0.0736685629	0.00378016
H	[ <sup>242</sup> Am]	0.1686687076	0.00397259	0.1611164143	0.00386775
I	[ <sup>242</sup> Cm]	0.1849589901	0.00305256	0.1793083124	0.00298431
S	-	34.06157919	0.15778665	34.280047124	0.15130481

For the development of the two surrogate models, two training datasets were generated using the LHS method on the extended SCIANTIX burnup module as discussed in Section 2.3, one for the SFR case of n = 8538 data points, and one for the LBE-FR case of n = 8579 data points. Apart from the two training datasets, five validation datasets were generated for the SFR case, and four validation datasets were generated for the LBE-FR case, with different sizes and variable limits for the purpose of assessing the predictive capability of the proposed surrogate model. The details of each dataset are shown in Table 2.9.

The performance of the helium production surrogate model for the SFR case is shown in Fig.2.31. The correlation exhibits the best performance for the training dataset (a) as is to be expected. For the datasets (b) to (e) the surrogate model exhibits good predictive capability, considering its wide applicability range in terms of irradiation conditions, with most points being concentrated around the 45° diagonal, and with RMSE ranging from 0.1986 to 0.2765 as shown in Table 2.10. The R<sup>2</sup> and R<sup>2</sup><sub>adj</sub> statistic metrics range from 0.5983 to 0.7123 indicating a good fit to the values produced from the SCIANTIX burnup module. Fig. 2.32 shows the performance of the surrogate model for the LBE-FR case, which exhibits a better fit with the generated datasets compared to the SFR case (Table 2.11).

The variance associated with the predicted values occurs due to the high number of input variable combinations which lead to different burnup values for each initial fuel composition. For higher number of data points in each dataset, better agreement is observed as a denser matrix of input values is generated.

**Table 2.9.** Generated datasets' specifications.

<b>Dataset</b>	<b>Number of data points, n</b>	<b>Fuel/Reactor Combination</b>	<b>Specifications</b>
(a)Training	8538	MOX/SFR	Full variable ranges
(b)Validation	10371	MOX/SFR	No Cm, No Np
(c)Validation	99445	MOX/SFR	Upper limit for $\dot{F} = 1.32 \cdot 10^{19}$
(d)Validation	86332	MOX/SFR	Full variable ranges
(e)Validation	9973	MOX/SFR	Constant O/M, $T_{\text{fuel}}$ , $\rho_{\text{fuel}}$
(f)Training	8579	MOX/LBE-FR	Full variable ranges
(g)Validation	84648	MOX/LBE-FR	No Am
(h)Validation	9968	MOX/LBE-FR	Constant Pu/HM = 20%
(i)Validation	313	MOX/LBE-FR	Constant Pu/HM = 50%

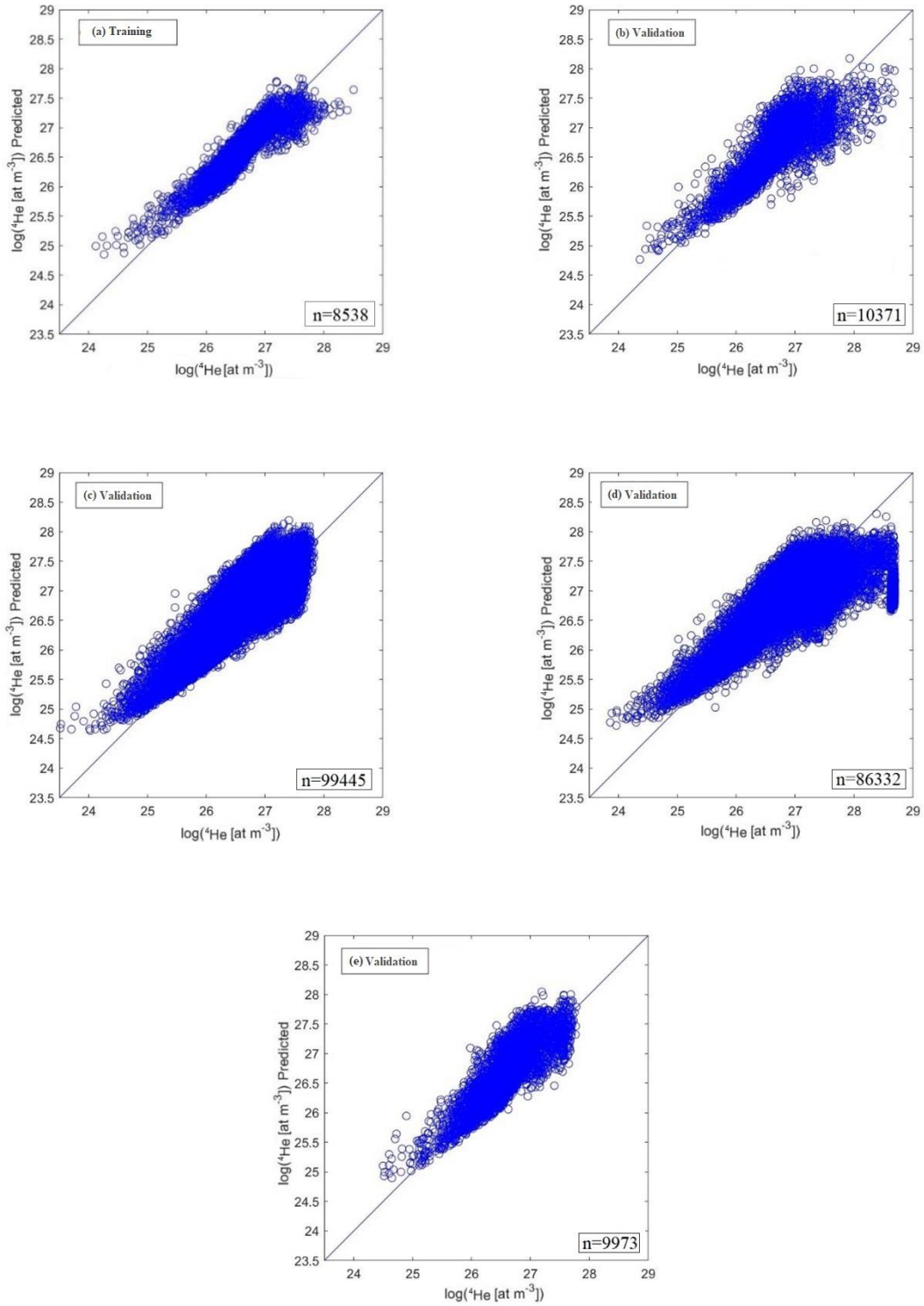


**Fig.2.31.** Evaluation of the proposed helium production surrogate model against the values calculated by SCIANTIX for five datasets in the SFR case, where (a) is the training dataset and (b) to (e) are validation datasets.

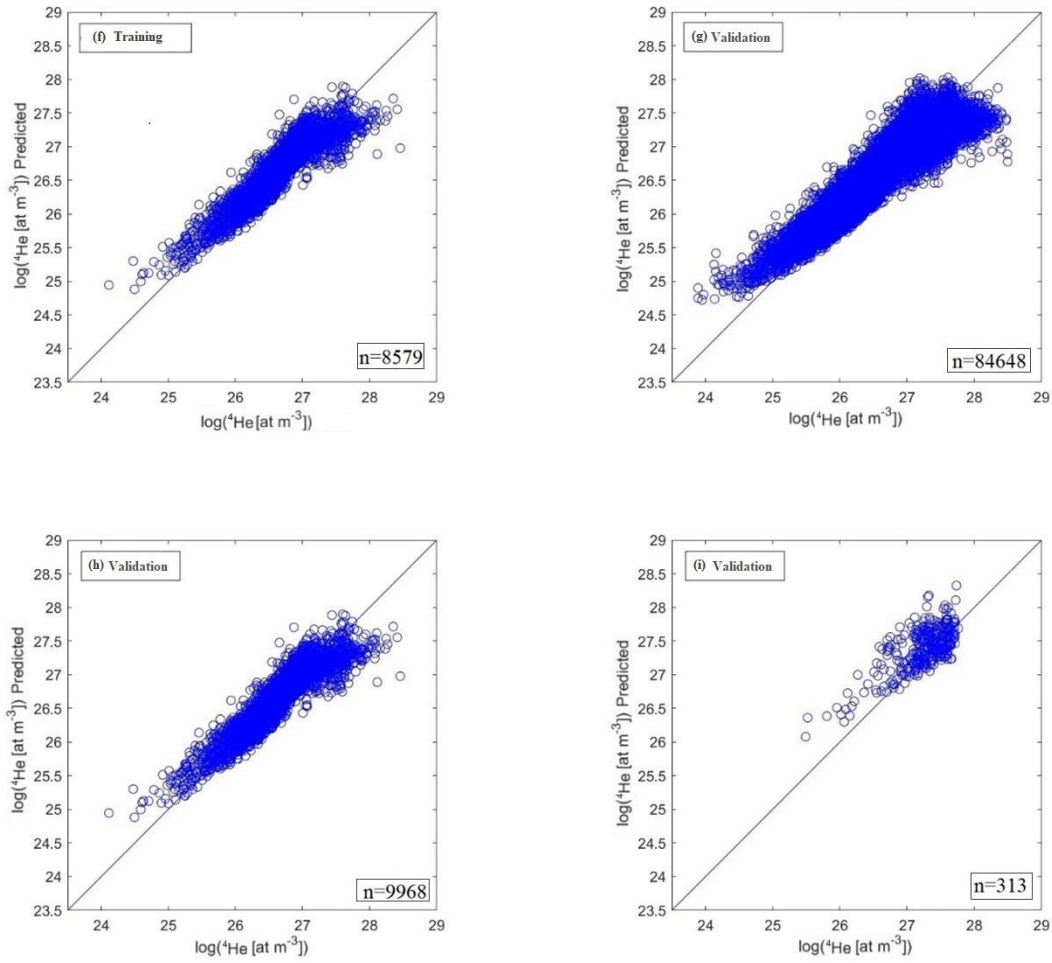


**Fig.2.32.** Evaluation of the proposed helium production surrogate model against the values calculated by SCIANTIX for four datasets in the LBE-FR case, where (f) is the training dataset and (g) to (i) are the validation datasets.

**Table 2.10.** Statistic validation metrics of the proposed helium production surrogate model for each dataset on the SFR case.

	n = 8538	n = 10371	n = 99445	n = 86332	n = 9973
Dataset	(a),(Training)	(b)	(c)	(d)	(e)
RMSE	0.165	0.2759	0.1986	0.2059	0.1976
R <sup>2</sup>	0.8123	0.6019	0.7106	0.6889	0.7085
R <sup>2</sup> adjusted	0.8122	0.6017	0.7104	0.6889	0.7083

**Table 2.11.** Statistic validation metrics of the proposed helium production surrogate model for each dataset on the LBE-FR case.

	n = 8579	n = 84648	n = 9968	n = 313
Dataset	(f),(Training)	(g)	(h)	(i)
RMSE	0.1486	0.1504	0.1818	0.3094
R <sup>2</sup>	0.8441	0.8455	0.7542	0.5136
R <sup>2</sup> adjusted	0.844	0.8455	0.754	0.5094

In addition to the surrogate model depicted in Eq. 2.10, an ordinary differential equation for the calculation of the helium production rate  $d[{}^4\text{He}]/dt$  is developed in this work by deriving the expression for the helium concentration correlation to obtain:

$$\frac{d[{}^4\text{He}]}{dt} = A \cdot t_{irr}^{A-1} 10^P$$

where P is given by:

$$P = [B \cdot \dot{F} + (C \cdot [\text{Pu}] + D \cdot [\text{Pu}]^2 + E \cdot [\text{Pu}]^3) + F \cdot \rho_{fuel} + G \cdot [{}^{241}\text{Am}] + H \cdot [{}^{242}\text{Am}] + I \cdot [{}^{242}\text{Cm}] + S] \quad (2.11)$$

### 3 Conclusions

In this work the SCIANTIX burnup module has been extended and verified for two fuel/reactor combinations, sodium-cooled fast reactor and lead-bismuth eutectic cooled fast reactor. The extension allows to simulate MOX fuels with minor actinide concentrations. The depletion calculations made by the model were compared to the high-fidelity results from the SERPENT depletion code, in terms of the root-mean square error metric. The extended burnup module is found to perform well in its whole definition range, i.e., burnup from 0 to 200 GWd/t<sub>HM</sub> and Pu/HM from 20 to 51%. Furthermore, the results were validated against data from the SUPERFACT-1 and SPHERE experimental campaigns and found to be within the benchmarked thresholds.

Using the extended burnup module, datasets were generated using the Latin hypercube sampling method with several input vectors covering a wide span of initial fuel compositions and thermophysical properties correlated to the production of helium in the fuel. Non-linear multivariate regression was performed to obtain two surrogate models corresponding to the sodium and lead-bismuth eutectic fast reactor cases, respectively. The direct use of these surrogate models enables entirely bypassing the need of a burnup module for the assessment of the helium production rate in the fuel, thus allowing for reduced computational time, which is of potential interest for fuel performance codes targeting efficient thermo-mechanic calculations.

The proposed surrogate models for helium production have been verified against secondary generated datasets and found to be satisfactorily reliable in the considered ranges of input variables. Additionally, a helium production rate ordinary differential equation is proposed, which is potentially convenient for implementation in e.g., multi-physics schemes.

A natural extension of the proposed approach of using a burnup module to derive a surrogate model for application in fuel performance codes is to tailor to a specific irradiation experiment or a reactor case. Such dedicated correlation can ease the development of new reactor design, since fast running and inherently stable simulation tools are key for accelerating the design process.

As for the surrogate models proposed in this work, which are available in SCIANTIX, future developments will include further extension of the burnup module towards a wider set of fuel/reactor combinations and including different fuel compositions such as minor actinide bearing MOX fuels.

## 4 References

- [1] Olander, D. R. *Fundamental aspects of nuclear reactor fuel elements*. United States: N. p., 1976. Web. doi:10.2172/7343826.
- [2] K. Shibata, T. Kawano, T. Nakagawa, O. Iwamoto, J. Katakura, T. Fukahori, S. Chiba, A. Hasegawa, T. Murata, H. Matsunobu, T. Ohsawa, Y. Nakajima, T. Yoshida, A. Zukeran, M. Kawai, M. Baba, M. Ishikawa, T. Asami, T. Watanabe, Y. Watanabe, M. Igashira, N. Yamamuro, H. Kitazawa, N. Yamano and H. Takano: "Japanese Evaluated Nuclear Data Library Version 3 Revision-3: JENDL-3.3," J. Nucl. Sci. Technol. 39, 1125 (2002).
- [3] Rider BF. *Compilation of fission product yields, NEDO-12154-3(C)*. California, USA: General Electric Co.; 1981.
- [4] D'Agata, E. et al., 2014. SPHERE: irradiation of sphere-pac fuel of U<sub>2</sub>PO<sub>8</sub> containing 3%. Nucl. Eng. Des. 275, 300–311.
- [5] L. Luzzi, T. Barani, B. Boer, L. Cognini, A. Del Nevo, M. Lainet, S. Lemehov, A. Magni, V. Marelle, B. Michel, D. Pizzocri, A. Schubert, P. Van Uffelen, M. Bertolus, Assessment of three European fuel performance codes against the SUPERFACT-1 fast reactor irradiation experiment, Nuclear Engineering and Technology, Volume 53, Issue 10, 2021, Pages 3367-3378, ISSN 1738-5733, <https://doi.org/10.1016/j.net.2021.04.010>.
- [6] D'Agata, E. et al., 2013. The results of the irradiation experiment MARIOS on americium transmutation. Ann. Nucl. Energy 62, 40–49.
- [7] K. Lassmann, TRANSURANUS: a fuel rod analysis code ready for use, J. Nucl. Mater. 188 (1992) 295e302, [https://doi.org/10.1016/0022-3115\(92\)90487-6](https://doi.org/10.1016/0022-3115(92)90487-6).
- [8] I.R. Birss, Helium production in reactor materials: Review paper, Journal of Nuclear Materials, Volume 34, Issue 3, 1970, Pages 241-259, ISSN 0022-3115, [https://doi.org/10.1016/0022-3115\(70\)90192-3](https://doi.org/10.1016/0022-3115(70)90192-3).
- [9] L.R. Greenwood, A new calculation of thermal neutron damage and helium production in nickel, Journal of Nuclear Materials, Volume 115, Issues 2–3, 1983, Pages 137-142, ISSN 0022-3115, [https://doi.org/10.1016/0022-3115\(83\)90302-1](https://doi.org/10.1016/0022-3115(83)90302-1).
- [10] Federici, E, Courcelle, A, Blanpain, P, and Cognon, H. *Helium production and behavior in nuclear oxide fuels during irradiation in LWR*. United States: N. p., 2007
- [11] Bell, M. J. "origen-2 Code." *ORNL-TM4397, Oak Ridge National Laboratories (ORNL)* (1973).
- [12] Poston, David I., and Holly R. Trellue. *Users manual, version 1.00 for MonteBurns, version 3.01*. No. LA-UR-98-2718. Los Alamos National Lab.(LANL), Los Alamos, NM (United States), 1998.
- [13] S. M. Bowman, M. D. DeHart, and C. V. Parks, "Validation of SCALE-4 for Burnup Credit Applications," Nuclear Technology, vol. 110, no. 1, pp. 53–70, 1995.
- [14] P. Van Uffelen, J. Hales, W. Li, G. Rossiter, R. Williamson, A review of fuel performance modelling, J. Nucl. Mater. 516 (2019) 373e412, <https://doi.org/10.1016/j.jnucmat.2018.12.037>.
- [15] K. Lassmann, The structure of fuel element codes, Nucl. Eng. Des. 57 (1980) 17e39, [https://doi.org/10.1016/0029-5493\(80\)90221-6](https://doi.org/10.1016/0029-5493(80)90221-6).
- [16] R.L. Williamson, J.D. Hales, S.R. Novascone, M.R. Tonks, D.R. Gaston, C.J. Permann, D. Andrs, R.C. Martineau, Multidimensional Multiphysics simulation of nuclear fuel behavior, J. Nucl. Mater. 423 (2012) 149e163, <https://doi.org/10.1016/j.jnucmat.2012.01.012>.
- [17] K. Lassmann, C. O'Carroll, J. van de Laar, C.T. Walker, The radial distribution of plutonium in high burnup UO<sub>2</sub> fuels, J. Nucl. Mater. 208 (3) (1994) 223e231.
- [18] Cechet, Alessandro & Altieri, S. & Barani, Tommaso & Cognini, L. & Lorenzi, Stefano & Magni, Alessio & Pizzocri, Davide & Luzzi, Lelio. (2021). A new burn-up module for application in fuel performance calculations targeting the helium production rate in (U,Pu)O<sub>2</sub> for fast reactors. Nuclear Engineering and Technology. 53. 1893-1908. 10.1016/j.net.2020.12.001.
- [19] C.B. Lee, D.H. Kim, J.S. Song, J.G. Bang, Y.H. Jung, RAPID model to predict radial burnup distribution in LWR UO<sub>2</sub> fuel, J. Nucl. Mater. 282 (2e3) (2000) 196e204.
- [20] S.Y. Kurchatov, V.V. Likhanskii, A.A. Sorokin, O.V. Khoruzhii, RTOP-code simulation of the radial distribution of heat release and plutonium isotope accumulation in high burnup oxide fuel, At. Energy 92 (4) (2002) 349e356.
- [21] A. Soba, A. Denis, Simulation with DIONISIO 1.0 of thermal and mechanical pellet-cladding interaction in nuclear fuel rods, J. Nucl. Mater. 374 (1e2) (2008) 32e43.

- [22] Hiroshi Akie, Isamu Sato, Motoe Suzuki, Hiroyuki Serizawa & Yasuo Arai (2013) Simple formula to evaluate helium production amount in fast reactor MA-containing MOX fuel and its accuracy, *Journal of Nuclear Science and Technology*, 50:1, 107-121, DOI: 10.1080/00223131.2013.750066
- [23] V. I. Tarasov, E. F. Mitenkova, N. V. Novikov. (2019) MFPR/R-Aided Modeling of Hydrogen and Helium Production in Nuclear Fuel. *Atomic Energy* 125:6, pages 370-375.
- [24] J. Leppaanen, M. Pusa, T. Viitanen, V. Valtavirta, T. Kaltiainenaho, The SERPENT Monte Carlo code: status, development and applications, in: in: SNA þ MC 2013 - Joint International Conference on Supercomputing in Nuclear Applications þ Monte Carlo, Paris, France, 27-31 October 2013, OECD/NEA, 2014
- [25] D. Pizzocri, T. Barani, and L. Luzzi, "SCIANTIX: A new open source multi-scale code for fission gas behaviour modelling designed for nuclear fuel performance codes," *Journal of Nuclear Materials*, p. 152042, 2020. [Online]. Available: <https://doi.org/10.1016/j.jnucmat.2020.152042>
- [26] D. Pizzocri, T. Barani, L. Luzzi, Coupling of TRANSURANUS with the SCIANTIX fission gas behaviour module, *Int. Work. "Towards Nucl. fuel Model. Var. React. types across Eur.* (2019).
- [27] Talou, T. Kawano, P.G. Young, M.B. Chadwick, R.E. MacFarlane, Improved evaluations of neutron-induced reactions on americium isotopes, *Nucl. Sci. Eng.* 155 (1) (2007) p84-95.
- [28] P. Botazzoli, Helium Production and Behaviour in LWR Oxide Nuclear Fuels, PhD Thesis, Politecnico di Milano, Italy, 2011.
- [29] K. Tasaka, J. Katakura, H. Ihara, T. Yoshida, S. Iijima, R. Nakasima, T. Nakagawa, H. Takano, JNDC Nuclear Data Library of Fission Products - Second Version, JAERI 1320, 1990.
- [30] S. Altieri, "A burnup meta-model for application in fuel performance codes: development and verification for MOX fuel in pressurized water reactors," MSc thesis, Politecnico di Milano, 2018.
- [31] A. Cechet, Modelling of helium behaviour in oxide nuclear fuels for fuel performance analysis, MSc. Thesis, Politecnico di Milano, Italy, 2019.
- [32] J. Leppänen, Serpent – a Continuous-energy Monte Carlo Reactor Physics Burnup Calculation Code – User’s Manual, 2015.
- [33] M. Pusa, Numerical Methods for Nuclear Fuel Burnup Calculations, 2013.
- [34] Jadot, F., et al. "ASTRID sodium cooled fast reactor: Program for improving in service inspection and repair." *2011 2nd International Conference on Advancements in Nuclear Instrumentation, Measurement Methods and their Applications*. IEEE, 2011.
- [35] Pietro Botazzoli, Lelio Luzzi, Stephane Brémier, Arndt Schubert, Paul Van Uffelen, Clive T. Walker, Wim Haeck, Wolfgang Goll, Extension and validation of the TRANSURANUS burn-up model for helium production in high burn-up LWR fuels, *Journal of Nuclear Materials*, Volume 419, Issues 1–3, 2011, Pages 329-338, ISSN 0022-3115, <https://doi.org/10.1016/j.jnucmat.2011.05.040>.
- [36] Mckay, M. & Beckman, Richard & Conover, William. (1979). A Comparison of Three Methods for Selecting Vales of Input Variables in the Analysis of Output From a Computer Code. *Technometrics*. 21. 239-245. 10.1080/00401706.1979.10489755.
- [37] US NRC (US Nuclear Regulatory Commission). Severe accident risks: an assessment for five US nuclear power plants. NUREG- 1150, vols. 1–3. Washington, DC: US Nuclear Regulatory Commission, Office of Nuclear Regulatory Research, Division of Systems Research; 1990–1991.
- [38] Breeding RJ, Helton JC, Gorham ED, Harper FT. Summary description of the methods used in the probabilistic risk assessments for NUREG-1150. *Nuclear Engng Des* 1992;135(1):1–27.
- [39] Breeding RJ, Helton JC, Murfin WB, Smith LN. Evaluation severe accident risks: Surry Unit 1. NUREG/CR-4551, SAND86-1309, vol. 3, Rev. 1. Albuquerque, NM: Sandia National Laboratories; 1990.
- [40] J.C. Helton, F.J. Davis, Latin hypercube sampling and the propagation of uncertainty in analyses of complex systems, *Reliability Engineering & System Safety*, Volume 81, Issue 1, 2003, Pages 23-69, ISSN 0951-8320, [https://doi.org/10.1016/S0951-8320\(03\)00058-9](https://doi.org/10.1016/S0951-8320(03)00058-9).
- [41] Giorgio Locatelli, Mauro Mancini, Nicola Todeschini, Generation IV nuclear reactors: Current status and future prospects, *Energy Policy*, Volume 61, 2013, Pages 1503-1520, ISSN 0301-4215, <https://doi.org/10.1016/j.enpol.2013.06.101>.
- [42] MathWorks, "MATLAB code", 2019. [Online]. Available: <https://uk.mathworks.com/products/matlab.html> .

- [44] JMP®, Version 16.1. SAS Institute Inc., Cary, NC, 1989–2021.
- [45] Glantz, Stanton A.; Slinker, B. K. (1990). *Primer of Applied Regression and Analysis of Variance*. McGraw-Hill. ISBN 978-0-07-023407-9.
- [37] Giorgio Locatelli, Mauro Mancini, Nicola Todeschini, Generation IV nuclear reactors: Current status and future prospects, *Energy Policy*, Volume 61, 2013, Pages 1503-1520, ISSN 0301-4215, <https://doi.org/10.1016/j.enpol.2013.06.101>.
- [38] D. Olander, Nuclear fuels – Present and future, *Journal of Nuclear Materials*, Volume 389, Issue 1, 2009, Pages 1-22, ISSN 0022-3115, <https://doi.org/10.1016/j.jnucmat.2009.01.297>.
- [39] J.-M. Bonnerot, Propriétés thermiques des oxydes mixtes d'uranium et de plutonium, PhD thesis, 1988.
- [40] Juan J Carbajo, Gradyon L Yoder, Sergey G Popov, Victor K Ivanov, A review of the thermophysical properties of MOX and UO2 fuels, *Journal of Nuclear Materials*, Volume 299, Issue 3, 2001, Pages 181-198, ISSN 0022-3115, [https://doi.org/10.1016/S0022-3115\(01\)00692-4](https://doi.org/10.1016/S0022-3115(01)00692-4).
- [41] D. Staicu et al., Preparing ESNII for HORIZON 2020 - Deliverable D7.3.4 - Characterization and measurement of properties of fresh TRABANT fuel, ESNII + Deliverable, 2017.

## A. APPENDIX A

Complete set of the Bateman equations implemented in the SCIANITX burnup module:

$$\begin{aligned} \frac{d[{}^4\text{He}]}{dt} = & \lambda_{\alpha,234\text{U}} [{}^{234}\text{U}] + \lambda_{\alpha,235\text{U}} [{}^{235}\text{U}] + \lambda_{\alpha,236\text{U}} [{}^{236}\text{U}] + \lambda_{\alpha,238\text{U}} [{}^{238}\text{U}] \\ & + \lambda_{\alpha,237\text{Np}} [{}^{237}\text{Np}] \\ & + \lambda_{\alpha,238\text{Pu}} [{}^{238}\text{Pu}] + \lambda_{\alpha,239\text{Pu}} [{}^{239}\text{Pu}] + \lambda_{\alpha,240\text{Pu}} [{}^{240}\text{Pu}] + \lambda_{\alpha,242\text{Pu}} [{}^{242}\text{Pu}] \\ & + \lambda_{\alpha,241\text{Am}} [{}^{241}\text{Am}] + \lambda_{\alpha,243\text{Am}} [{}^{243}\text{Am}] \\ & + \lambda_{\alpha,242\text{Cm}} [{}^{242}\text{Cm}] + \lambda_{\alpha,243\text{Cm}} [{}^{243}\text{Cm}] + \lambda_{\alpha,244\text{Cm}} [{}^{244}\text{Cm}] + \lambda_{\alpha,245\text{Cm}} [{}^{245}\text{Cm}] + \sigma_{n,\alpha}{}^{16}\text{O} \varphi [{}^{16}\text{O}] + y_{TF} \dot{F} \end{aligned} \quad (\text{A.1})$$

$$\frac{d[{}^{234}\text{U}]}{dt} = \lambda_{\beta,234\text{Pa}} [{}^{234}\text{Pa}] + \lambda_{\alpha,238\text{Pu}} [{}^{238}\text{Pu}] - \lambda_{\alpha,234\text{U}} [{}^{234}\text{U}] + \sigma_{n,2n}{}^{235}\text{U} \varphi [{}^{235}\text{U}] - \sigma_{\alpha}{}^{234}\text{U} \varphi [{}^{234}\text{U}] \quad (\text{A.2})$$

$$\frac{d[{}^{235}\text{U}]}{dt} = \lambda_{\alpha,239\text{Pu}} [{}^{239}\text{Pu}] - \lambda_{\alpha,236\text{U}} [{}^{236}\text{U}] + \sigma_c{}^{234}\text{U} \varphi [{}^{234}\text{U}] - \sigma_{\alpha}{}^{235}\text{U} \varphi [{}^{235}\text{U}] - \sigma_{n,2n}{}^{235}\text{U} \varphi [{}^{235}\text{U}] \quad (\text{A.3})$$

$$\frac{d[{}^{236}\text{U}]}{dt} = \lambda_{\alpha,240\text{Pu}} [{}^{240}\text{Pu}] + \lambda_{\alpha,235\text{U}} [{}^{235}\text{U}] + \sigma_c{}^{235}\text{U} \varphi [{}^{235}\text{U}] - \sigma_{\alpha}{}^{236}\text{U} \varphi [{}^{236}\text{U}] + \sigma_{n,3n}{}^{238}\text{U} \varphi [{}^{238}\text{U}] \quad (\text{A.3})$$

$$\frac{d[{}^{237}\text{U}]}{dt} = \sigma_c{}^{236}\text{U} \varphi [{}^{236}\text{U}] - \lambda_{\beta,237\text{U}} [{}^{237}\text{U}] - \sigma_{\alpha}{}^{237}\text{U} \varphi [{}^{237}\text{U}] + \sigma_{n,2n}{}^{238}\text{U} \varphi [{}^{238}\text{U}] \quad (\text{A.4})$$

$$\begin{aligned} \frac{d[{}^{238}\text{U}]}{dt} = & \lambda_{\alpha,242\text{Pu}} [{}^{242}\text{Pu}] - \lambda_{\alpha,238\text{U}} [{}^{238}\text{U}] + \sigma_c{}^{237}\text{U} \varphi [{}^{237}\text{U}] - \sigma_{\alpha}{}^{238}\text{U} \varphi [{}^{238}\text{U}] - \sigma_{n,2n}{}^{238}\text{U} \varphi [{}^{238}\text{U}] \\ & + \sigma_{n,3n}{}^{238}\text{U} \varphi [{}^{238}\text{U}] \end{aligned} \quad (\text{A.5})$$

$$\frac{d[{}^{237}\text{Np}]}{dt} = \lambda_{\beta,237\text{U}} [{}^{237}\text{U}] + \lambda_{\alpha,241\text{Am}} [{}^{241}\text{Am}] - \lambda_{\alpha,237\text{Np}} [{}^{237}\text{Np}] - \sigma_{\alpha}{}^{237}\text{Np} \varphi [{}^{237}\text{Np}] \quad (\text{A.6})$$

$$\frac{d[{}^{238}\text{Np}]}{dt} = \sigma_c{}^{237}\text{Np} \varphi [{}^{237}\text{Np}] - \sigma_{\alpha}{}^{238}\text{Np} \varphi [{}^{238}\text{Np}] \quad (\text{A.7})$$

$$\begin{aligned} \frac{d[{}^{239}\text{Np}]}{dt} = & \sigma_c{}^{238}\text{U} \varphi [{}^{238}\text{U}] + \lambda_{\alpha,243\text{Am}} [{}^{243}\text{Am}] + \sigma_c{}^{238}\text{Np} \varphi [{}^{238}\text{Np}] - \sigma_{\alpha}{}^{239}\text{Np} \varphi [{}^{239}\text{Np}] \\ & - \lambda_{\beta,239\text{Np}} [{}^{239}\text{Np}] \end{aligned} \quad (\text{A.8})$$

$$\frac{d[{}^{238}\text{Pu}]}{dt} = \lambda_{\beta^{238}\text{Np}} \varphi [{}^{238}\text{Np}] + \lambda_{\alpha^{242}\text{Cm}} [{}^{242}\text{Cm}] - \lambda_{\alpha^{238}\text{Pu}} [{}^{238}\text{Pu}] - \sigma_{\alpha^{238}\text{Pu}} \varphi [{}^{238}\text{Pu}] \quad (\text{A.9})$$

$$\begin{aligned} \frac{d[{}^{239}\text{Pu}]}{dt} = & \sigma_{c^{238}\text{Pu}} \varphi [{}^{238}\text{Pu}] + \lambda_{\beta^{239}\text{Np}} [{}^{239}\text{Np}] + \lambda_{\alpha^{243}\text{Cm}} [{}^{243}\text{Cm}] \\ & - \sigma_{\alpha^{239}\text{Pu}} \varphi [{}^{239}\text{Pu}] - \lambda_{\alpha^{239}\text{Pu}} [{}^{239}\text{Pu}] \end{aligned} \quad (\text{A.10})$$

$$\begin{aligned} \frac{d[{}^{240}\text{Pu}]}{dt} = & \lambda_{\alpha^{244}\text{Cm}} [{}^{244}\text{Cm}] + \sigma_{c^{239}\text{Pu}} \varphi [{}^{239}\text{Pu}] + \sigma_{c^{239}\text{Np}} \varphi [{}^{239}\text{Np}] - \lambda_{\alpha^{240}\text{Pu}} [{}^{240}\text{Pu}] \\ & - \sigma_{\alpha^{240}\text{Pu}} \varphi [{}^{240}\text{Pu}] \end{aligned} \quad (\text{A.11})$$

$$\frac{d[{}^{241}\text{Pu}]}{dt} = \lambda_{\alpha^{245}\text{Cm}} [{}^{245}\text{Cm}] + \sigma_{c^{240}\text{Pu}} \varphi [{}^{240}\text{Pu}] - \lambda_{\beta^{241}\text{Pu}} [{}^{241}\text{Pu}] - \sigma_{\alpha^{241}\text{Pu}} \varphi [{}^{241}\text{Pu}] \quad (\text{A.12})$$

$$\frac{d[{}^{242}\text{Pu}]}{dt} = \lambda_{EC^{242}\text{Am}} [{}^{242}\text{Am}] + \sigma_{c^{241}\text{Pu}} \varphi [{}^{241}\text{Pu}] - \lambda_{\alpha^{242}\text{Pu}} [{}^{242}\text{Pu}] - \sigma_{\alpha^{242}\text{Pu}} \varphi [{}^{242}\text{Pu}] \quad (\text{A.13})$$

$$\frac{d[{}^{243}\text{Pu}]}{dt} = \sigma_{c^{242}\text{Pu}} \varphi [{}^{242}\text{Pu}] - \lambda_{\beta^{243}\text{Pu}} [{}^{243}\text{Pu}] - \sigma_{\alpha^{243}\text{Pu}} \varphi [{}^{243}\text{Pu}] \quad (\text{A.14})$$

$$\frac{d[{}^{241}\text{Am}]}{dt} = \lambda_{\beta^{241}\text{Pu}} [{}^{241}\text{Pu}] - \lambda_{\alpha^{241}\text{Am}} [{}^{241}\text{Am}] - \sigma_{\alpha^{241}\text{Am}} \varphi [{}^{241}\text{Am}] \quad (\text{A.15})$$

$$\begin{aligned} \frac{d[{}^{242}\text{Am}]}{dt} = & \sigma_{c, BR^{241}\text{Am}} \varphi [{}^{241}\text{Am}] + \lambda_{IT^{242m}\text{Am}} [{}^{242m}\text{Am}] - \sigma_{\alpha^{242}\text{Am}} \varphi [{}^{242}\text{Am}] - \lambda_{\beta^{242}\text{Am}} [{}^{242m}\text{Am}] \\ & + \lambda_{EC^{242}\text{Am}} [{}^{242}\text{Am}] \end{aligned} \quad (\text{A.16})$$

$$\frac{d[{}^{242m}\text{Am}]}{dt} = \sigma_{c, BR^{241}\text{Am}} (1 - BR_{Am^{241}}) \varphi [{}^{241}\text{Am}] - \sigma_{\alpha^{242m}\text{Am}} \varphi [{}^{242m}\text{Am}] - \lambda_{IT^{242m}\text{Am}} [{}^{242m}\text{Am}] \quad (\text{A.17})$$

$$\begin{aligned} \frac{d[{}^{243}\text{Am}]}{dt} = & \sigma_{c^{242}\text{Am}} \varphi [{}^{242}\text{Am}] + \sigma_{c^{242m}\text{Am}} \varphi [{}^{242m}\text{Am}] - \sigma_{\alpha^{243}\text{Am}} \varphi [{}^{243}\text{Am}] + \lambda_{\beta^{243}\text{Pu}} [{}^{243}\text{Pu}] \\ & - \lambda_{\alpha^{243}\text{Am}} [{}^{243}\text{Am}] \end{aligned} \quad (\text{A.18})$$

$$\frac{d[{}^{244}\text{Am}]}{dt} = \sigma_{c^{243}\text{Am}} \varphi [{}^{243}\text{Am}] - \lambda_{\beta^{244}\text{Am}} [{}^{244}\text{Am}] - \sigma_{\alpha^{241}\text{Am}} \varphi [{}^{241}\text{Am}] \quad (\text{A.19})$$

$$\frac{d[{}^{242}\text{Cm}]}{dt} = \lambda_{\beta^{244}\text{Am}} [{}^{244}\text{Am}] - \lambda_{\alpha^{242}\text{Cm}} [{}^{242}\text{Cm}] - \sigma_{\alpha^{242}\text{Cm}} \varphi [{}^{242}\text{Cm}] \quad (\text{A.20})$$

$$\frac{d[{}^{243}\text{Cm}]}{dt} = \sigma_{c^{242}\text{Cm}} \varphi [{}^{242}\text{Cm}] - \lambda_{\alpha^{243}\text{Cm}} [{}^{243}\text{Cm}] - \sigma_{\alpha^{243}\text{Cm}} \varphi [{}^{243}\text{Cm}] \quad (\text{A.21})$$

$$\frac{d[{}^{244}\text{Cm}]}{dt} = \lambda_{\beta^{244}\text{Am}} [{}^{244}\text{Am}] + \sigma_{c^{243}\text{Cm}} \varphi [{}^{243}\text{Cm}] - \lambda_{\alpha^{244}\text{Cm}} [{}^{244}\text{Cm}] - \sigma_{\alpha^{244}\text{Cm}} \varphi [{}^{244}\text{Cm}] \quad (\text{A.22})$$

$$\frac{d[{}^{245}\text{Cm}]}{dt} = \sigma_{c^{244}\text{Cm}} \varphi [{}^{244}\text{Cm}] + \sigma_{c^{244}\text{Am}} \varphi [{}^{244}\text{Am}] - \lambda_{\alpha^{245}\text{Cm}} [{}^{245}\text{Cm}] - \sigma_{\alpha^{245}\text{Cm}} \varphi [{}^{245}\text{Cm}] \quad (\text{A.23})$$

## 5 Abstract in lingua italiana

La produzione di elio nella matrice del combustibile nucleare durante l'irraggiamento è un fenomeno di primaria importanza nelle fasi di progetto e di operazione del combustibile nei reattori di quarta generazione, in quanto fattore limitante per quanto riguarda la pressurizzazione interna della barretta. In questo lavoro si propone un modello surrogato per la produzione di elio, sviluppato sulla base dell'analisi statistica di set di dati prodotti artificialmente dal modulo di burnup SCIANITIX. Tale modulo è stato esteso come parte di questo lavoro di tesi, verificato rispetto ai risultati ad alta fedeltà del codice Monte Carlo SERPENT, e confrontato con i risultati sperimentali degli esperimenti SUPERFACT-1 e SPHERE. Il modello surrogato ottenuto permette il calcolo della produzione di elio in combustibili per reattori veloci caratterizzati dalla presenza di attinidi minori (MA), in funzione della densità del combustibile, della densità di fissione del reattore e del tempo di irraggiamento. Il modello surrogato ha l'obiettivo di ridurre drasticamente i tempi di calcolo facilitandone l'utilizzo ingegneristico nell'ambito dei codici di performance termomeccanica della barretta di combustibile.

Parole chiave: Combustibile MOX, Attinidi Minori, Produzione di Elio, Reattori Veloci, Generazione IV

## 6 Acknowledgements

For the completion of this work, I would like to acknowledge and thank my supervisor, Prof. Lelio Luzzi, who accepted me in the Nuclear Reactors' Group and presented me with the unique opportunity of working on this topic.

I would like to thank my co-supervisor Davide Pizzocri, for his clear guidance, invaluable advice, and constant availability.

I would like to thank Alessio Magni, for his insightful comments and helpful feedback and Giovanni Zullo, for his crucial help on technical matters.

I would also like to give special thanks to my family, without whose indispensable help and tireless support, none of this would have come to fruition.

---

This work has received funding from the Euratom research and training programme 2019-2020 under grant agreement No 945077 (PATRICIA Project).

